Optical spectroscopy of a complete sample of southern 2-Jy radio sources*

C. N. Tadhunter,¹ R. Morganti,² S. di Serego Alighieri,³ R. A. E. Fosbury⁴† and I. J. Danziger⁵

- ¹Department of Physics, University of Sheffield, Sheffield S3 7RH
- ² Istituto di Radioastronomia, via Irnerio 46, I-40126 Bologna, Italy
- ³Osservatorio Astrofisico di Arcetri, Largo E. Fermi 5, I-50125, Firenze, Italy
- ⁴Space Telescope–European Coordinating Facility, European Southern Observatory, Karl-Schwarzschild–Straβe-2, D-8046, Garching bei München, Germany

Accepted 1993 February 12. Received 1993 February 4; in original form 1992 October 5

ABSTRACT

We present optical spectra for a complete sample of radio galaxies and quasars comprising all sources from the Wall & Peacock 2.7-GHz sample with redshifts z < 0.7 and declinations $\delta < +10^{\circ}$; this sample is complete down to a flux density of 2 Jy. Although not all of the 2-Jy sources have spectroscopic redshifts, we argue that most of the unidentified objects are at high redshifts and that our z < 0.7 sample is largely complete. The optical data will be analysed in a future paper.

Key words: galaxies: active – galaxies: distances and redshifts – quasars: emission lines.

1 INTRODUCTION

It has been clear since the discovery of the optical counterparts of extragalactic radio sources in the 1950s and 1960s that the narrow optical emission-line properties are strongly correlated with the radio continuum properties (e.g. Schmidt 1965; Hine & Longair 1979). Starting with the work of Yee & Oke (1978), several quantitative investigations have attempted to understand the physical basis of the radio/ optical correlation (Baum et al. 1988; Baum & Heckman 1989a,b; Rawlings et al. 1989; Saunders et al. 1989; Morganti, Ulrich & Tadhunter 1992). All these studies show a strong formal correlation between the emission-line luminosity and the radio power. In addition, Rawlings & Saunders (1991) have shown that the emission-line luminosity is even more strongly correlated with the bulk jet power than with the radio power. The results suggest that the optical/radio correlation arises, at least in part, from the increase in photoionizing flux with radio power, although it cannot be ruled out that some of the correlation arises because another property (e.g. gas covering fraction) changes with radio power or redshift. Also, it is uncertain whether the correlations depend on how the radio sources were selected (all the past studies have used samples selected at low radio frequencies), or whether they depend on the detailed radio structure (e.g. whether the sources are compact: see Morganti et al. 1992).

Orientation effects, as embodied in the unified schemes for radio sources (e.g. Orr & Browne 1982; Barthel 1989), may also influence the observed optical/radio correlation. There is debate about whether the narrow emission-line properties are independent of orientation: whether quasars – viewed from the direction of the radio axis in the unified schemes – have the same narrow emission-line properties (such as luminosities) as radio galaxies – viewed perpendicular to the radio axis in the unified schemes. There is already some evidence that the emission-line luminosities are smaller in the radio galaxies than in the quasars (Jackson & Browne 1990) for a given radio luminosity, but further detailed observations of the emission-line regions in radio sources are required to determine whether this represents definitive evidence against the unified schemes.

Motivated by the current lack of understanding about the relationship between radio and optical properties in powerful radio sources, and also by the sparsity of good optical data for southern radio sources, we have embarked on a major optical spectroscopic and radio survey of a large sample of southern radio galaxies and quasars. In this, the

⁵European Southern Observatory, Karl-Schwarzschild-Straße-2, D-8046, Garching bei München, Germany

^{*}This work is based on observations made at the European Southern Observatory, La Silla, Chile.

[†]Affiliated to the Astrophysics Division, Space Science Department, European Space Agency.

1000 C. N. Tadhunter et al.

first of a series of papers concerned with our survey, we present the optical spectra (Paper I). Future papers will present the radio data (Paper II: Morganti, Killeen & Tadhunter 1993), new redshifts and optical identifications (Paper III: di Serego Alighieri et al., in preparation) and the analysis of the optical and radio results (Paper IV: Tadhunter et al., in preparation).

2 SAMPLE SELECTION AND OBSERVING STRATEGY

Our aim was to obtain homogeneous spectroscopic data in the optical waveband for a complete subset of the Wall & Peacock (1985) 2.7-GHz sample (hereafter WP85), selected using the following criteria: declinations $\delta < 10^{\circ}$ and redshifts z < 0.7. The WP85 sample and, by implication, our subsample are complete down to a flux density of 2 Jy.

The redshift limit was set by instrumental limitations, given that we wanted to obtain accurate measurements of the $[O \, \textsc{iii}] \lambda 5007$ line. At higher redshifts this important diagnostic line is shifted into a region of severe fringing/poor sensitivity for the instruments we were using.

In the WP85 catalogue there are 67 objects with known redshifts that fulfil the above criteria. However, since we wished our sample of z < 0.7 sources to be as complete as possible, and also wished to improve on the completeness of the optical identifications and redshifts of the WP85 sample of radio sources, we also elected to obtain spectra of all the 47 sources with declinations $\delta < 10^\circ$ for which no spectroscopic redshift (and sometimes no optical identification) is given in WP85 (for these sources WP85 give a redshift estimated from the magnitude). The new optical identifications and redshifts are the subject of Paper III, but the objects for which our new spectroscopic redshift is less than 0.7 are obviously included in the complete sample and therefore discussed in the following. The completeness of our z < 0.7 sample is discussed in Section 5.

The advantages of this sample for studies of the emissionline/radio correlation are:

- (1) the sample is selected at relatively high radio frequencies and therefore it forms a complement to the low-frequency samples used for this type of work in the past;
- (2) the sample spans a wide range in extended radio luminosity, which is useful for investigating the nature of the optical/radio correlation;
- (3) the sample contains a relatively high proportion of compact steep-spectrum (CSS) radio sources, and it is of great interest to compare the properties of the CSS objects with those of the more extended double radio sources.

Our aim in planning the observations was to obtain homogeneous spectroscopic data with good flux calibration for all the sample members. Along with measurements of the $[O\ m]\lambda 5007$ emission-line fluxes and luminosities, we planned to cover the rest wavelength range $3400-5200\ Å$ for all the sample members. This was to allow us to measure the $[O\ n]\lambda 3727/[O\ m]\lambda 5007$ ionization diagnostic, and to obtain a good baseline in the continuum.

A further important feature of our observing strategy was to attempt to obtain observations with wide (>2.5 arcsec) slits for all our target objects. This was in order to minimize seeing slit losses, to guard against small pointing errors, to

minimize the effects of differential atmospheric refraction, and to attempt to include as much as possible of the (possibly extended) nuclear narrow-line region.

In this paper we have set $H_0 = 50$ km s⁻¹ Mpc⁻¹ and $a_0 = 0$.

3 OBSERVATIONS

Here we present the new observations for the objects that are included in the complete sample (i.e. z < 0.7). The log of the observations for these objects is presented in Table 1. The observations were completed in four runs using the ESO 3.6-m and 2.2-m telescopes at La Silla, Chile: in 1989 March, April, and December, and 1990 July.

Where possible, we observed the brighter objects $(m_{\nu} < 17)$ with the Boller & Chivens spectrograph on the ESO/MPI 2.2-m telescope (Heydari-Melayeri, Jarvis & Gillotte 1989), and the fainter objects with the ESO Faint Object Spectrograph and Camera (EFOSC, Melnick, Dekker & D'Odorico 1989) on the ESO 3.6-m telescope. However, some objects observed with the 2.2-m were found to be fainter than expected and were subsequently re-observed with the 3.6-m.

Some of the objects were observed using two different slitwidths (listed in Table 1). As mentioned before, this was done to check the accuracy of the flux measurements and slit losses (see Section 6).

The conditions were photometrically stable on all four of the observing runs, and comparisons between the flux calibration standard stars within individual nights and runs show that the flux calibrations are good, in absolute terms, to within 20 per cent. Typically, two or three observations of secondary flux calibration stars were obtained each night.

The data were reduced using the FIGARO software package at the Cambridge node of Starlink, and using the MIDAS package at ESO headquarters. The reduction followed standard procedures and included subtraction of bias, flatfielding, correction for fringing, wavelength calibration, correction for atmospheric extinction using the standard ESO extinction curve (Schwarz & Melnick 1989), sky subtraction and flux calibration. No attempt was made to correct for detailed atmospheric absorption features (e.g. atmospheric A and B bands).

Following the data reduction, the one-dimensional nuclear spectra were extracted from the 2D data frames prior to the measurement of the emission-line fluxes. In the spatial direction the length of the extraction apertures was varied to include all the obvious line emission associated with the core of the galaxy (i.e. associated with the bright continuum source). In a few rare cases, there was significant line emission from bright clouds off-nucleus (e.g. 2250 – 41 and 2152-69). These cases are noted in Section 7. For most objects, however, the emission lines were found to be concentrated around the nuclear continuum source, in agreement with the imaging results of Baum et al. (1988). We are confident, therefore, that we have included the bulk of the line emission within the slit for most objects. Even in extreme cases like 2152-69 or 2250-41, the correction to the total $[O III] \lambda 5007$ emission-line flux is only ~50 per cent if the extranuclear regions are included.

The line fluxes were measured by fitting Gaussian profiles to the emission line using the FIGARO routine GAUSS. For the

low-luminosity radio sources in our sample, the emission lines often had small equivalent widths and, in such cases, we subtracted template elliptical galaxy spectra prior to the measurement of the emission-line fluxes.

We note the following effects which may influence the quality of our data.

- (1) Fringing in the red (especially EFOSC frames). The thinned RCA CCD used in EFOSC for our observations produces significant fringing effects at wavelengths $\lambda > 7000$ Å. Division of the data frames by suitable flat-field exposures reduces the fringe amplitude to about 5-15 per cent, but does not eliminate the fringes entirely. The main negative consequence of the fringing is to reduce the accuracy of the sky subtraction in a part of the spectrum in which the sky subtraction is particularly important. Overall, continuum features in our spectra cannot be trusted at wavelengths $\lambda > 7000$ Å, but the effect on the accuracy of our emission-line fluxes is not serious and is limited to the amplitude of the residual fringes (i.e. <15 per cent loss in accuracy).
- (2) The change in metric aperture size as a function of redshift. The extraction apertures correspond to much larger swathes of the galaxies at high redshifts (most of the galaxies included in the slit) than at low redshifts (only the immediate surrounds of the nuclei of the galaxies included). As already mentioned above, we do not believe that this is a serious problem in most cases, because the emission-line regions are generally concentrated on the nuclei (see also Baum et al. 1988) and we have deliberately made wide-slit observations to counter this effect. The problem is likely to be most serious for the nearby objects, with emission-line regions of relatively low surface brightness. For most such cases, however, we have only been able to derive upper limits on the [O III] flux. Since these upper limits are conservative, it is unlikely that the aperture effect will seriously affect our conclusions about the radio/optical correlation.

Taking into account all the possible sources of error, we believe that most of our $[O III] \lambda 5007$ emission-line fluxes are accurate to within 30 per cent. In the rare cases in which our slit has missed bright, off-nuclear emission-line regions, the error might approach 50 per cent.

4 DETECTION LIMITS

Not all of our target objects were detected in the $[O\,\textsc{iii}]\lambda5007$ emission line. The sources without $[O\,\textsc{iii}]$ detections fall into two broad categories: radio sources at low redshifts and with low radio luminosities, which none the less have bright, extended stellar continua, and optically very faint radio sources which are presumably at much higher redshifts (see below).

The detection limit is not uniform with redshift and depends on the emission line under consideration. The following factors affect the detectability of an emission line.

(1) The instrumental sensitivity. The instrumental sensitivity is poor at the extreme red end of the spectrum ($\lambda > 8500 \,\text{Å}$), and this may make it difficult to detect weak [O III] emission in objects with z > 0.7. The instrumental sensitivity is also particularly poor at wavelengths $\lambda < 4000 \,\text{Å}$ (observed, not rest wavelength), where the response of the

CCD detector is dropping rapidly. This is evident from the noise in the continuum spectra of many of the low-redshift objects presented in Fig. 1. The poor blue response has the consequence that it is particularly difficult to detect the important $[O \, \pi] \, \lambda \, 3727$ line in many of the low-redshift objects.

- (2) The relative strength of the continuum. For typical radio galaxy continuum brightnesses, a given $[O\,\textsc{iii}]\lambda5007$ flux corresponds to a much larger equivalent width at high redshifts than at low redshifts, and in this sense it is easier to detect the emission lines against the continuum at high redshifts than at low redshifts. For many of the low-redshift objects, the relatively strong and highly structured stellar continuum makes it difficult to detect weak $[O\,\textsc{iii}]$ emission, even if attempts are made to subtract a continuum template. Similarly, the strong blue continuum in some quasars makes the relatively weak $[O\,\textsc{ii}]\lambda3727$ feature difficult to detect.
- (3) The sky background. This is more important at the red end of the spectrum ($\lambda > 7000 \,\text{Å}$) where there are several night sky emission bands than in the blue. It therefore mainly affects the detectability of $[O \,\textsc{iii}] \, \lambda 5007$ in the higher redshift objects.

Although the sky will have an important effect on the $[O\ m]$ detectability at higher redshifts, we believe that up to a redshift of about 0.75 the general detectability of emission lines (that is, the ability to detect any emission line in a given source) will improve as the redshift increases. This is because the $[O\ m]$ emission line becomes much easier to detect at high redshifts, and, for a given emission-line flux, the ability to detect emission lines against the stellar continuum also improves (see point 2 above). For the exposure times typical of our survey we believe that, beyond z > 0.2, we would detect all sources with $[O\ m]\ \lambda 5007$ or $[O\ m]\ \lambda 3727$ emission-line fluxes above 5×10^{-16} erg cm⁻² s⁻¹.

For the lower redshift radio sources in which we fail to detect $[O \, \text{III}] \lambda 5007$, we have set an upper limit on the strength of this line of 6σ , where σ is the noise in the template-subtracted continuum for a 50-Å bin centred on a rest wavelength of 5007 Å. We have not attempted to set upper limits for the strength of $[O \, \text{II}]$ in the low-luminosity radio sources, because the noise in the continuum at those shorter wavelengths is much larger (see Fig. 1), and the limit would not be very meaningful. Nevertheless, we have measured upper limits for the $[O \, \text{II}]$ in the quasars.

5 COMPLETENESS OF SAMPLE

In this section we discuss the completeness of our z < 0.7 sample. The final list of the 87 objects included in the 'complete sample' (together with some characteristics of the objects) is given in Table 2. In this table we list the most accurate positions for all the objects (for epoch 1950.0). These are usually VLA or ATCA radio positions of the core (see Paper II for details) for which the accuracy ranges between 0.1 and 0.3 arcsec. For all the sources the optical position was also determined using sky maps extracted from the digitized Schmidt plates available at the Space Telescope Science Institute (Lasker et al. 1990). The astrometric information necessary to obtain good optical positions is provided in the headers of the maps themselves. The accuracy of these positions is in general about 0.5 arscec and they agree, within the errors, with the estimated radio core

Table 1. Details of the observations.

Object	Other Name	Grism*/ λ range(Å)	Slit width	Exp. time	Telescope	Period
		v range(v)	arcsec	s		
0023 - 26	OB-238	B300	2.0,5.0	900,300	3.6	Dec89
0034 - 01	3C15	B300	3.0	600	3.6	July90
		3650-6200	2,4	1200,300	2.2	Dec89
0035 - 02	3C17	B300	2.0,5.0	600,180	3.6	Dec89
0038 + 09	3C18	B300	2.0,5.0	600,180	3.6	Dec89
0039 44		B300,R300	5.0	2x300	3.6	July90
0043 — 42		B300	5.0	600	3.6	July90
0045 - 25	NGC253	3650-6200 3650-6200	2,4 2	900,300 600	2.2 2.2	Dec89
0045 - 25 $0055 - 01$	3C29	3600-7000	3.0	1800	2.2	Dec89 July90
	0020	3650-6200	2,4	900,300	2.2	Dec89
		6030-8610	2,4	1800,300	2.2	Dec89
0105 - 16	3C32	R300,B300	2.0,2.0	1200,1200	3.6	Dec89
0117 - 15	3C38	B300,R300	2.0,2.0	1800,1200	3.6	Dec89
0123 - 01	3C40	3650-6200	2,4	600,180	2.2	Dec89
0131 - 36	NGC612	3600-7000	3.0	1800	2.2	July90
		3650-6200	2,4	600,180	2.2	Dec89
0159 — 11	3C57	R300	5.0	300	3.6	July90
0010 10	0.530	6030-8610	2,4	1200,300	2.2	Dec89
0213 - 13	3C62	B300	3.0	600	3.6	July90
0235 — 19 0240 — 00	OD-159 NGC1068	2xR300,B300 3650-6200	5.0,3.0,3.0	300,900,600	3.6	July90
0240 - 00 $0252 - 71$	NGC1008	B300	2,4 2.0	300,60 900	2.2 3.6	Dec89 Dec89
0255 + 05	3C75	3650-6200	2,4	600,180	2.2	Dec89
0305 + 03	3C78	3650-6200	2,4	600,180	2.2	Dec89
0320 - 37	ForA	3650-6200	2,4	300,120	2.2	Dec89
0325 + 02	3C88	3650-6200	2	300	2.2	Dec89
0403 - 13	OF-105	6030-8610	2,4	1800,300	2.2	Dec89
0404 + 03	3C105	B300	2.0	900	3.6	Dec89
0405 - 12	OF-109	3650-6200	2,4	900,300	2.2	Dec89
0409 — 75		2xB300,R300	2.0	1800,400,1800	3.6	Dec89
0427 - 53		3650-6200	2x2,4	2x900,240	2.2	Dec89
0430 + 05	3C120	B300	2,5	300,180	3.6	March89
0442 - 28 $0453 - 20$	OF-271 OF-289	3650-6200	2,4	1800,600 600	2.2 2.2	Dec89 Dec89
0433 - 20 $0620 - 52$	OF-209	3650-6200 3600-7000	2,5	1200,900,300	2.2	March89
0625 - 53		3600-7000	2,5	2x900,300	2.2	March89
0625 - 35	OH-342	3600-7000	2,5	2x900,300	2.2	March89
0637 - 75		B300,R300	1.5,2.5	2x600	3.6	March89
		R300	2,5	1200,180,300		
0736 + 01	OI-61	B300	1.5,5	1200,600,300	3.6	March89
0806 — 10	3C195	B300	2.5,5	2x1200,180	3.6	March89
==		O150	1.5	1800,2x1200	4	
0842 - 75	07.000	R300	2.5,5	2x1200,300	3.6	March89
0859 - 25	OJ-299	R300	1.5,5	1200,300	3.6	March89
0915 — 11	HydA,3C218	B300	1.5	600		M1-00
1136 - 13	OM-161	3600-7000 R300	2,5 2.5,5	2x1200,300 1200,600,180	2.2 3.6	March89 March89
1150 - 10 $1151 - 34$	OM-386	3600-7000	3.0,5.0	1200,300	2.2	March89
	3	B300	2.0	1200	3.6	March89
1216 + 06	3C270	3600-7000	2,5	2x600,300	2.2	March89
1226 + 02	3C273	3600-7000	2,5	2x300	2.2	March89
1246 - 41	NGC4696	3600-7000	2,5	1200,600,300	2.2	March89
1251 - 12	3C278	3600-7000	2,5	1200,600,300	2.2	March89
1253 - 05	3C279	R300	1.5	900,600	3.6	March89
1306 - 09	OP-10	R300	1.5	1200	3.6	March89
1318 - 43	NGC5090	3600-7000	2,5	2x600,300	2.2	March89
1333 - 33	IC4296	3600-7000	2,5	2x600,300	2.2	March89
1355 - 41 $1510 - 08$	OR-107	3600-7000 B300	2,5	2x1800,300	2.2	March89 March89
1510 - 08 $1514 + 07$	3C317	3600-7000	1.5,5 2,5	900,600,180 1200,300	3.6 2.2	March89
1514 - 24		3600-7000		1200,300 1200,1800,2x300	2.2	March89
			-,0	,		

Table 1 - continued

Object	Other Name	Grism*/	Slit width	Exp. time	Telescope	Period
•		$\lambda \text{ range}(\text{\AA})$	arcsec	s		
1547 - 79		B300,R300	2.0	1200,1200	3.6	March89,July90
		R300	5	300		
1549 - 79		B300	2,5	900,300	3.6	March89,July90
1602 + 01	3C327.1	R300	1.5,5	2x1200,300	3.6	March89
		B300	2	600		
1637 - 77		3600-7000	2.5,5	1200,900,300	2.2	March89
1648 + 05	HerA	B300	2	2x900,300	3.6	March89
1717 - 00	3C353	3600-7000	3,5	2x1800,600	2.2	March89
1733 - 56		3600-7000	2.5,5	1800,300	2.2	March89
1814 - 63		B300	1.5,3	2x600,180	3.6	Apr89
1839 - 48		B300	1.5,3	2x600,180	3.6	Apr89
1932 - 46		B300	1.5,3	600,180	3.6	Apr89
1938 - 15	OV-164	2xR300,B300	2.0,5.0,5.0	1200,300,300	3.6	July90
1949 + 02	3C403	3600-7000	3.0,5.0	1800,600	2.2	July90
1954 — 55		3600-7000	3.0	900	2.2	July90
		2xB300	2.0	2x600	3.6	July90
1954 - 38		2xR300	2.0,5.0	900,300	3.6	July90
2058 - 28	OW-297.8	3600-7000	3.0,5.0	1200,300	2.2	July90
2104 - 25	OX-208	3600-7000	3.0,5.0	1800,600	2.2	July90
2128 - 12	OX-148	R300,B300	2x5.0	600,300	3.6	July90
2135 - 14	OX-158	3600-7000	3.0,5.0	1800,300	2.2	July90
2135 - 20	OX-20	2xR300	3.0,5.0	2x300	3.6	July90
		R300,B300	3.0,5.0	900,300	3.6	July90
2152 - 69)	R300,B300	2.0	2x1200	3.6	July90
2203 - 18	OY-106	R300,B300	2.0,5.0	1200,300	3.6	July90
2211 - 17	3C444	B300	3.0	1200	3.6	July90
2243 - 12	OY-172.6	2xR300	5.0,3.0	300,600	3.6	July90
2250 41		R300,B300	5.0,3.0	300,600	3.6	July90
		2xB300,O150	2x2.0,1.5	2x1200,900	3.6	July90
2314 + 03	3C459	3600-7000	3.0,5.0	1800,600	2.2	July90
2345 - 16	3	2xR300	5.0,3.0	2x600	3.6	July90

^{*} λ range for the grism used at the 3.6-m: B300 = 3600-7000 Å; R300 = 5600-9900 Å; O150 = 5000-7000 Å.

positions. These optical positions are given in Table 2 for the objects for which no radio core was observed. In the few cases for which no new radio or optical positions are available, we give the radio position from WP85.

All the information about the objects with z > 0.7, more details about the new identifications, and new redshifts will be given in Paper III.

5.1 Objects with previously measured redshifts

We made spectroscopic observations of 58 out of the 67 objects that have z < 0.7 and $\delta < +10^{\circ}$ in WP85. Most of these objects were without good measurements of the emission-line fluxes prior to our survey. For one of them, 0.743 - 6.7, we found that the redshift is 1.51 instead of 0.395, as given by WP85. This object was therefore excluded from the complete sample. Of the remaining nine sources, eight had adequate spectroscopic data in the literature (see Table 3).

The only object not observed in our survey which is also without good emission-line fluxes in the literature is 1322-42 (Centaurus A). This object is a special case, because its proximity makes it extremely difficult to measure

integrated emission-line fluxes without a time-consuming programme of narrow-band imaging or spectroscopy with several slit positions.

5.2 Objects without previously measured redshifts

Of the 47 sources in the catalogue of WP85 with $\delta < 10^\circ$ and no spectroscopic redshift, six objects have new published redshifts (two of them, 1602+01 and 1733-56, have z < 0.7). We set out to get spectroscopic redshifts of the remaining 41 sources, and we actually observed 38 sources. The three sources that we did not observe (0008-42, 1308-22 and 2150-52) are all faint optically $(m_V > 21.5)$ or classified as empty fields, and are extremely unlikely to have z < 0.7. We obtained new redshifts for 27 of the 38 sources that we did observe (see Paper III). Since 19 of the new redshifts are less than 0.7, the final 'complete sample' consists of 87 objects.

The 11 objects for which we have failed to identify recognizable features in our optical spectra have some common features.

(1) They are generally faint $(m_v > 20.5)$ and, for most, WP85 have estimated high redshifts (z > 0.7) on the basis of

1004 C. N. Tadhunter et al.

the observed correlation between redshift and apparent magnitude for radio galaxies.

(2) Their radio structures are generally compact – many are unresolved with the VLA B/C array at 6 cm (see also Paper II and Paper III). The small size is another possible

indication that they are distant. Furthermore, their radio positions are accurate, and it is unlikely that they have a wrong optical identification.

(3) If they were at z < 0.7, then their emission-line fluxes would be unusually small ($[O \text{ III}] \lambda 5007$ and

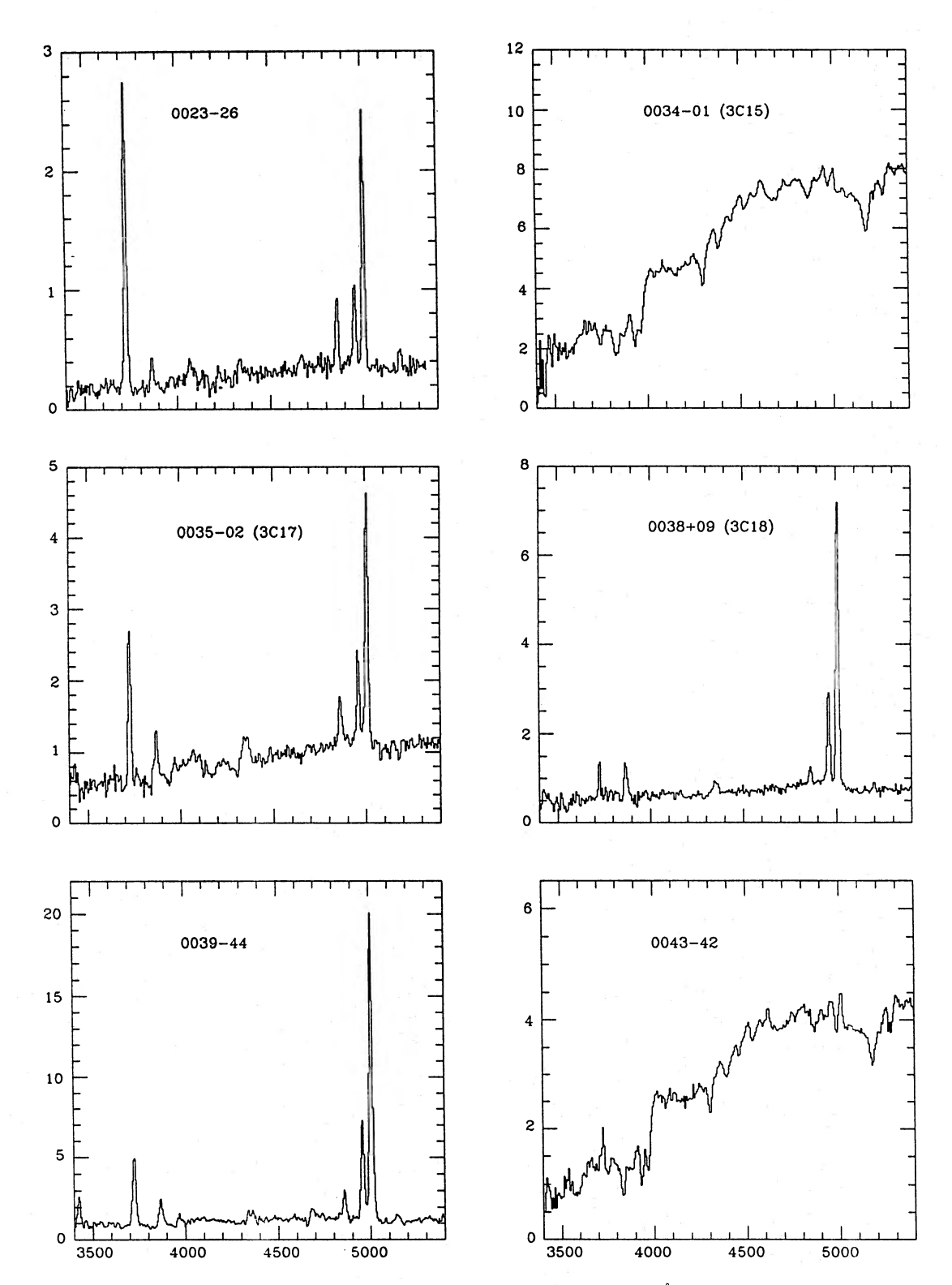


Figure 1. Spectra of all the objects observed in the survey with z < 0.7. The wavelengths are in Å and the flux scale is in units of 10^{-16} erg cm⁻² s⁻¹ Å⁻¹. The spectra have been shifted in wavelength to the rest frames of the host galaxies.

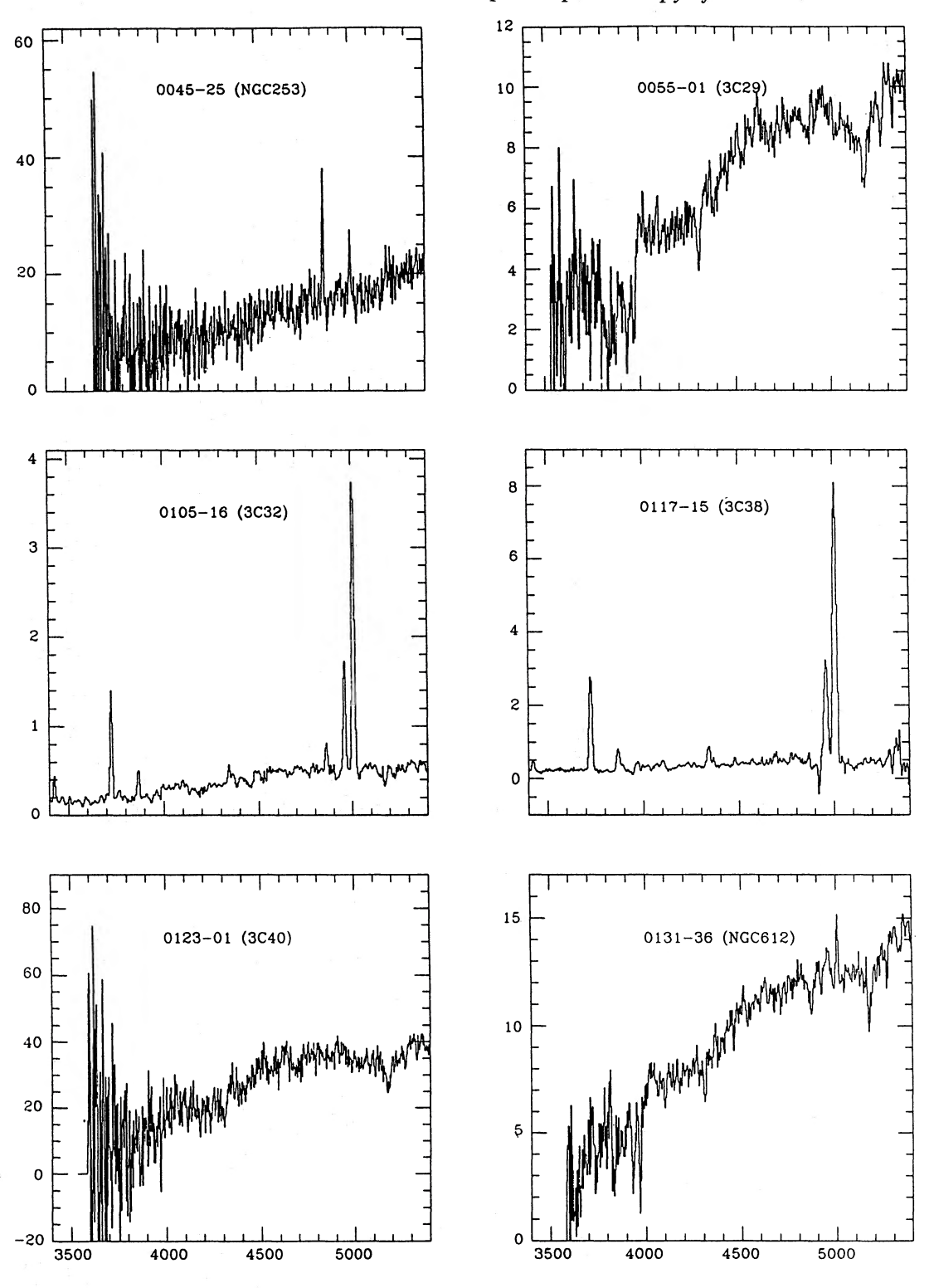


Figure 1 - continued

 $[O\,II]\lambda 3727 < 5 \times 10^{-16}$ erg cm⁻² s⁻¹; see Section 4), and they would fall off the correlation between emission-line luminosity and radio power which has been established for radio galaxies (Baum & Heckman 1989a; Rawlings et al. 1989; Morganti et al. 1992).

It appears most likely, therefore, that the majority of the unknown redshifts are high and that our z < 0.7 sample is largely complete. The alternative hypothesis is that there is a class of compact steep-spectrum radio sources which have unusually low optical continua and emission-line luminosi-

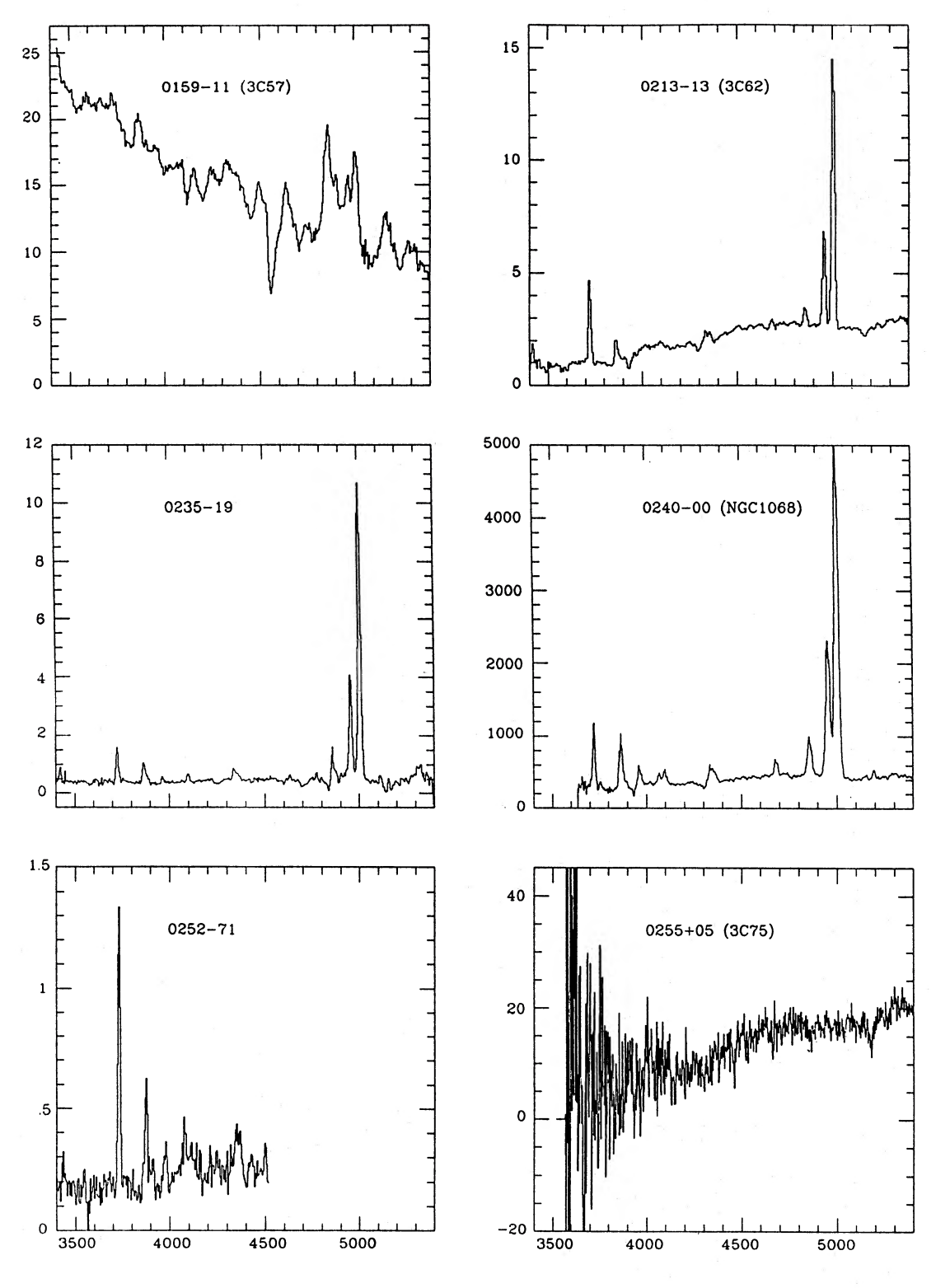


Figure 1 - continued

ties. This is not completely out of the question, since some sources that fall well below the correlation between emission-line luminosity and radio power have been found (e.g. Hercules A), but we regard as unlikely the possibility that there is a substantial population of such objects.

If we are pessimistic and assume that 30 per cent of the unknown redshifts are actually less than 0.7, and that we have failed to identify them because the emission-line fluxes are small, then our z < 0.7 sample would still be complete at the 95 per cent level.

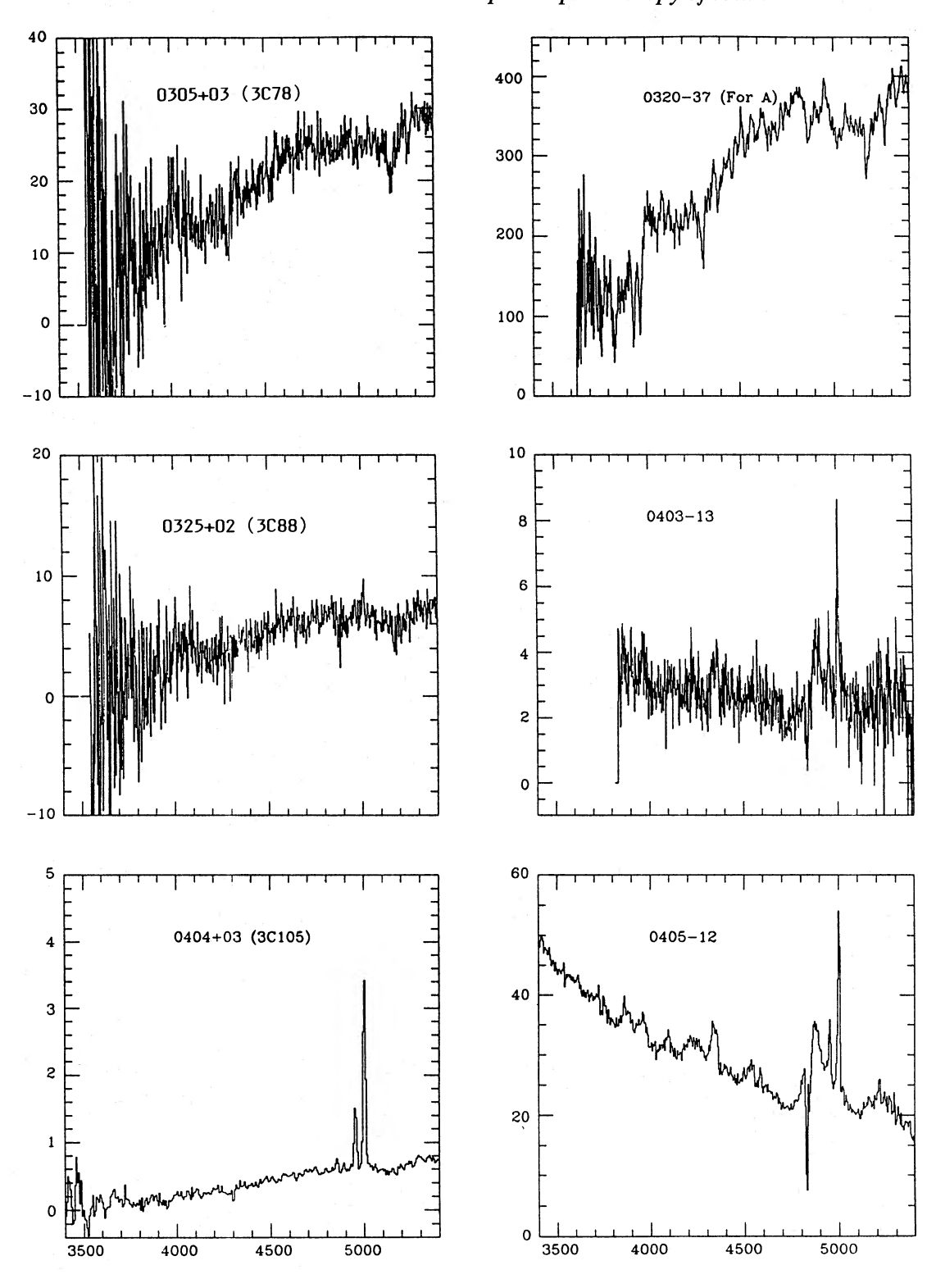


Figure 1 - continued

6 PRESENTATION OF THE DATA

Eight of the objects in our sample already had good published spectra and were not re-observed. These are listed with literature references in Table 3. The spectra for all the

remaining sources of the complete sample (except Cen A) are shown in Fig. 1.

Table 4 lists $[O \, \text{III}] \lambda 5007$ line fluxes, or upper limits, for all the sources in the complete sample. They represent the line fluxes for the widest slit observation for each object. We also

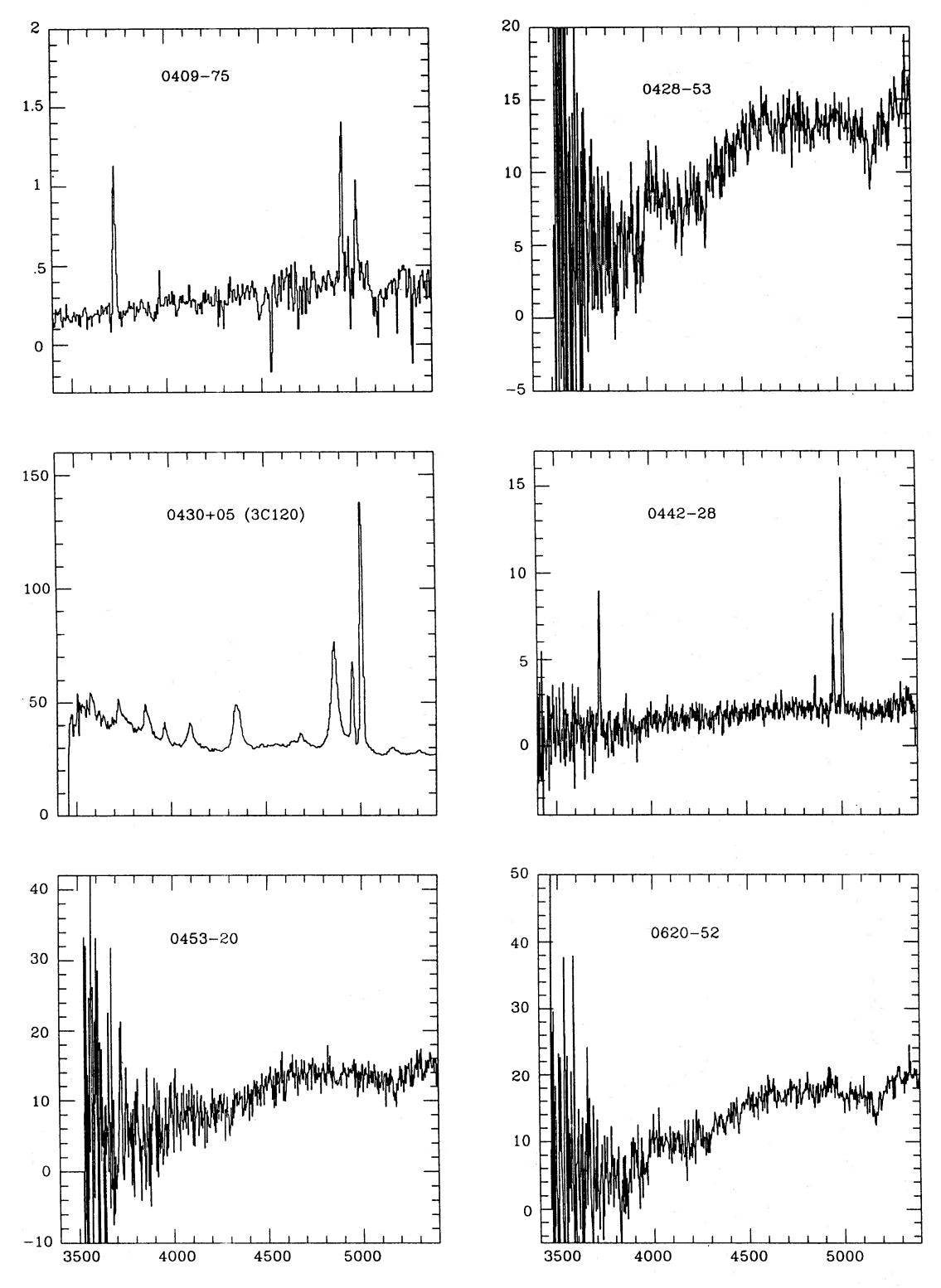


Figure 1 - continued

list the measured values for the $[O \,\textsc{ii}] \lambda 3727/[O \,\textsc{iii}] \lambda 5007$, $[O \,\textsc{iii}] \lambda 5007/H\beta$ emission-line diagnostics. The emission-line luminosities in the table have been calculated assuming that $H_0 = 50 \,\text{km s}^{-1} \,\text{Mpc}^{-1}$ and $q_0 = 0$. No attempt has been made to correct the fluxes or luminosities for the effects of interstellar extinction, either Galactic or extrinsic, although

all the objects with galactic latitude $|b| < 25^{\circ}$ are flagged in Table 4 (note that the WP85 catalogue includes only sources with $|b| > 10^{\circ}$).

We succeeded in obtaining wide-slit (typically 3-5 arcsec) observations for most sources in the sample, and additional narrow-slit (typically 1.5-2.5 arcsec) observations for many

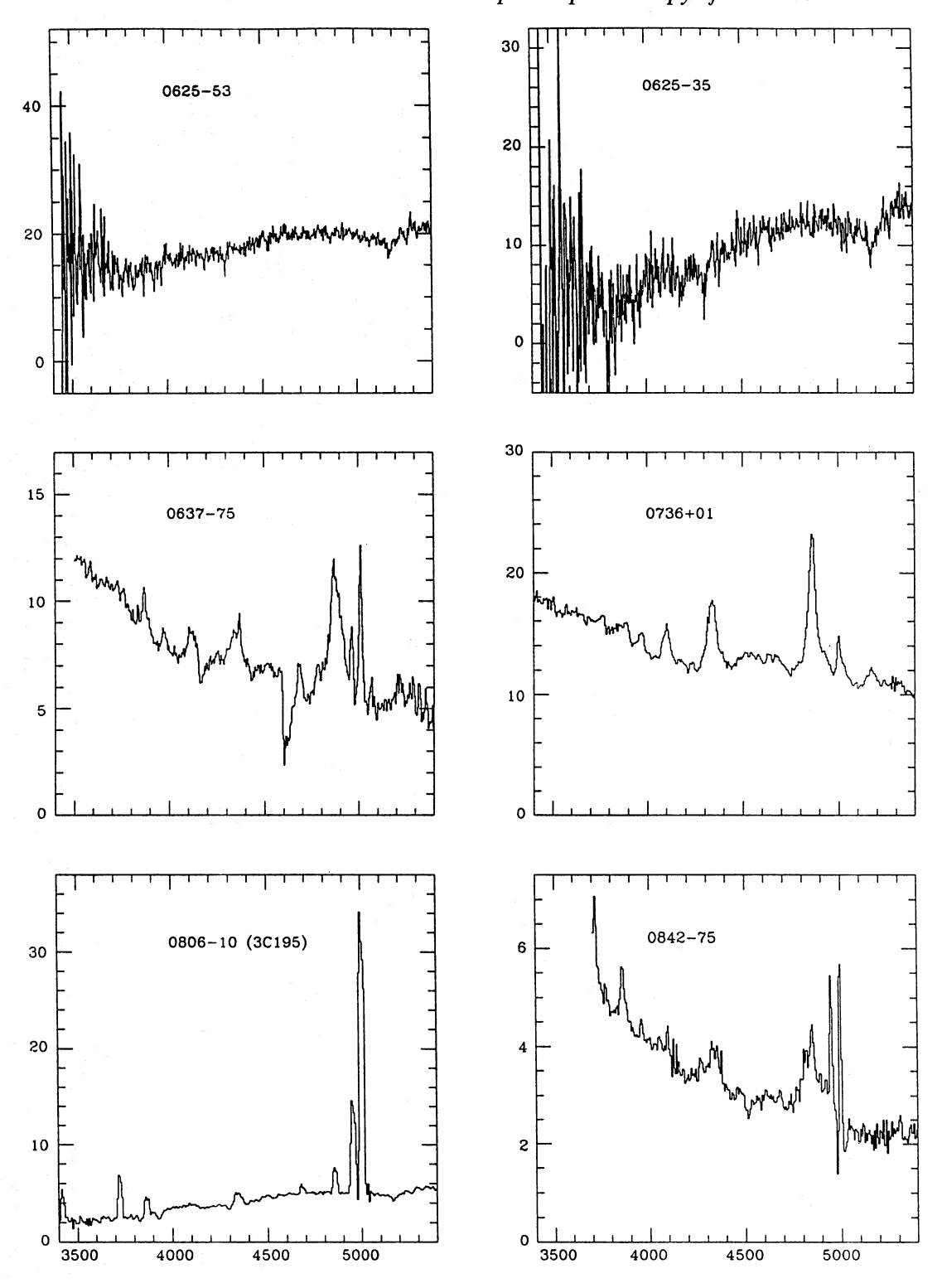


Figure 1 - continued

(see Table 1). Due to the lack of time, where both wide- and narrow-slit observations were made, the wide-slit observations have short integration times (typically 300 s). In some such cases – particularly for observations made with the 2.2-m telescope – the 'wide-slit' spectra are too noisy to give

reliable line fluxes, and we quote the narrow-slit fluxes in Table 4. To give an impression of the slit losses for the narrow-slit observations, Fig. 2 shows a histogram of the ratio between the wide- and the narrow-slit fluxes for the objects for which good measurements in both cases were

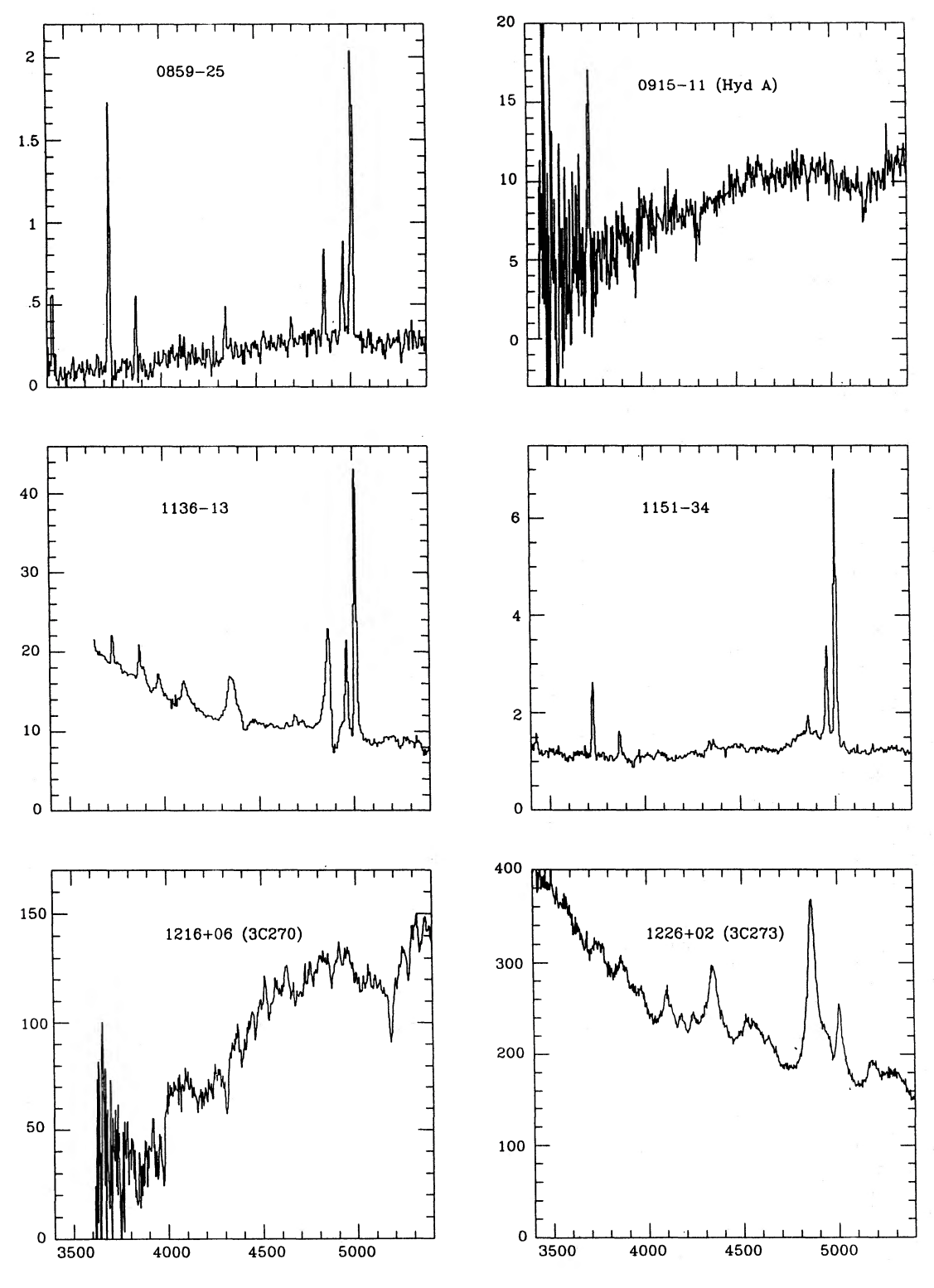


Figure 1 - continued

obtained (the values are listed in column 4 of Table 4). It is clear that the slit losses for narrow-slit observations are of order 10-50 per cent of the [O III] flux and up to a factor of 2 in extreme cases.

7 DETAILS OF INDIVIDUAL OBJECTS

0023–26. The optical spectrum of this compact steep-spectrum (CSS) radio source is of intermediate ionization with relatively strong lines of $[O II] \lambda 3727$ and $[N I] \lambda 5200$.

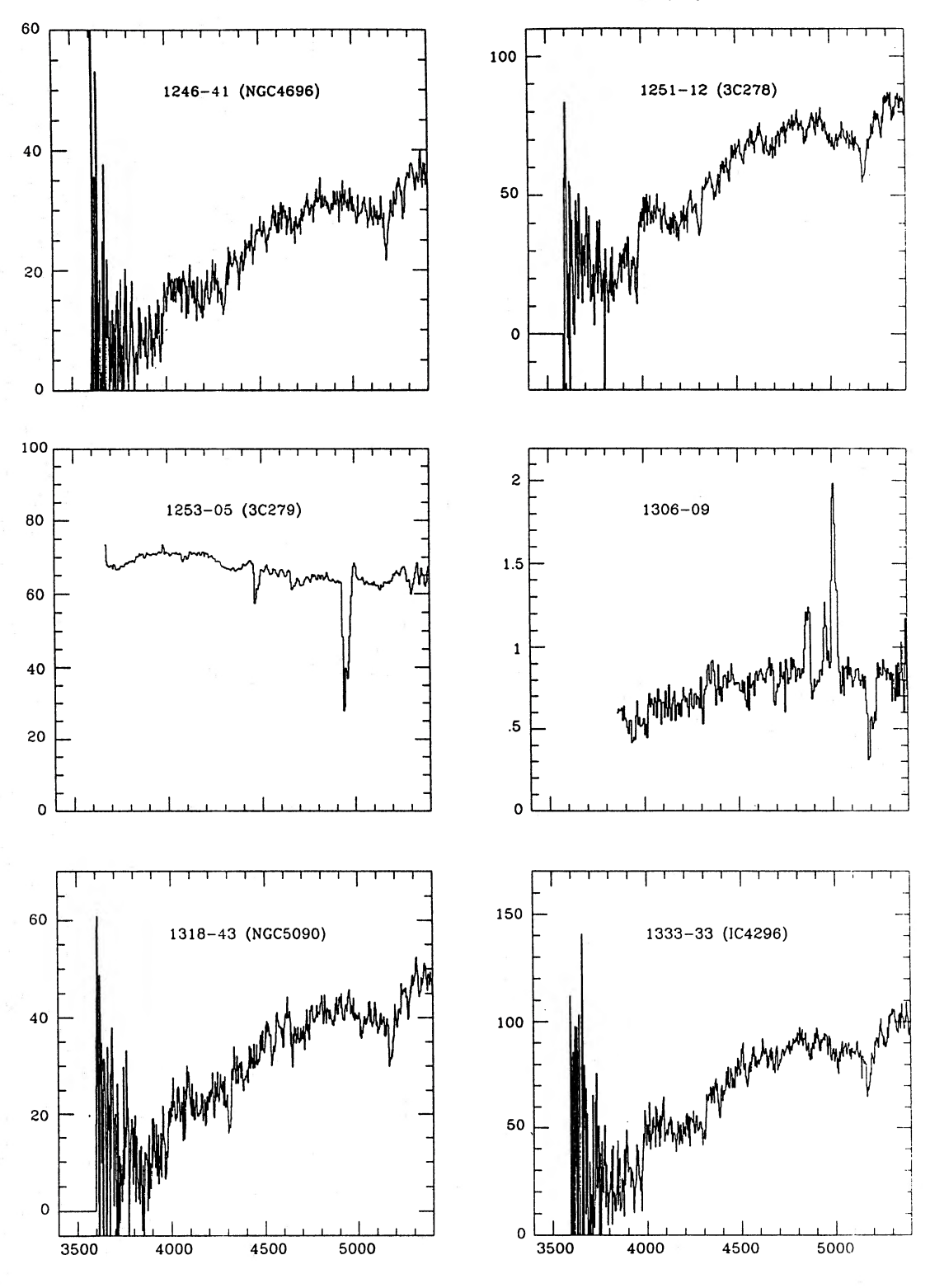


Figure 1 - continued

No stellar absorption features are detected (but the signal-to-noise ratio is low). The $[O\,\pi]$ emission may be slightly extended.

0034 – 01 (3C 15). Weak $[O \text{ III}] \lambda 5007$ is detected in this object. The continuum shows absorption features typical of

early-type galaxies. A difference of a few arcsec between the radio and the optical positions was found.

0035–02 (3C 17). Rich emission-line spectrum with hints of broad wings to the H β line. Ca II H absorption line is detected. The emission lines may be slightly extended.

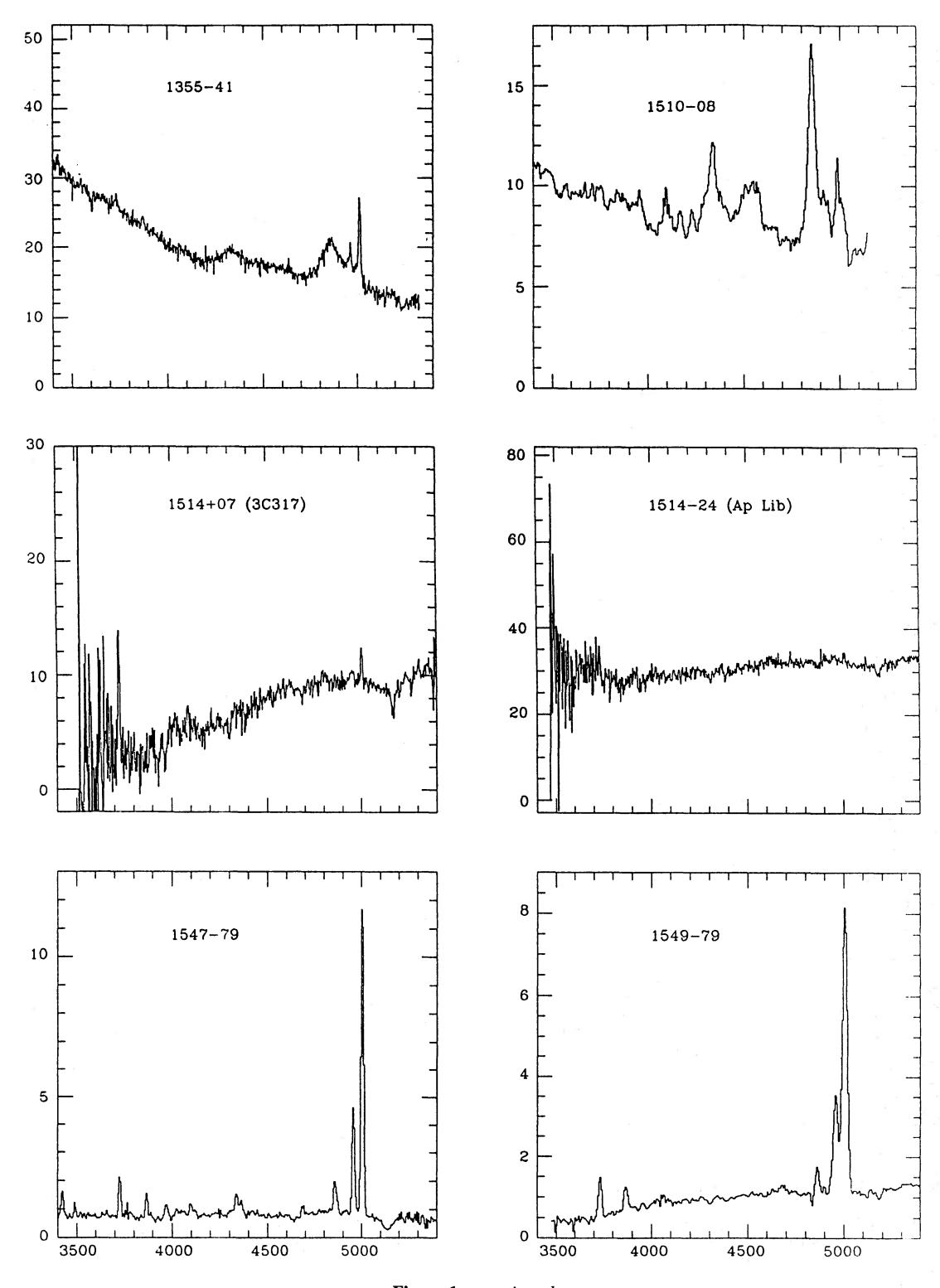


Figure 1 – continued

0038+09 (3C 18). Rich emission-line spectrum, with extremely high ionization state and hints of broad wings to the H β line. There are no clear detections of stellar absorption features. The emission lines may be slightly extended.

0039 – 44. Rich, high-ionization emission-line spectrum. There are no clear detections of stellar absorption features.

0043–42. Weak $[O II] \lambda 3727$ and $[O III] \lambda 5007$ emission lines are detected. The continuum spectrum is typical of early-type galaxies.

0045-25 (NGC 253). Narrow H β and [O III] λ 5007 emission lines have been detected from the nucleus of this starburst galaxy. No stellar absorption features have been

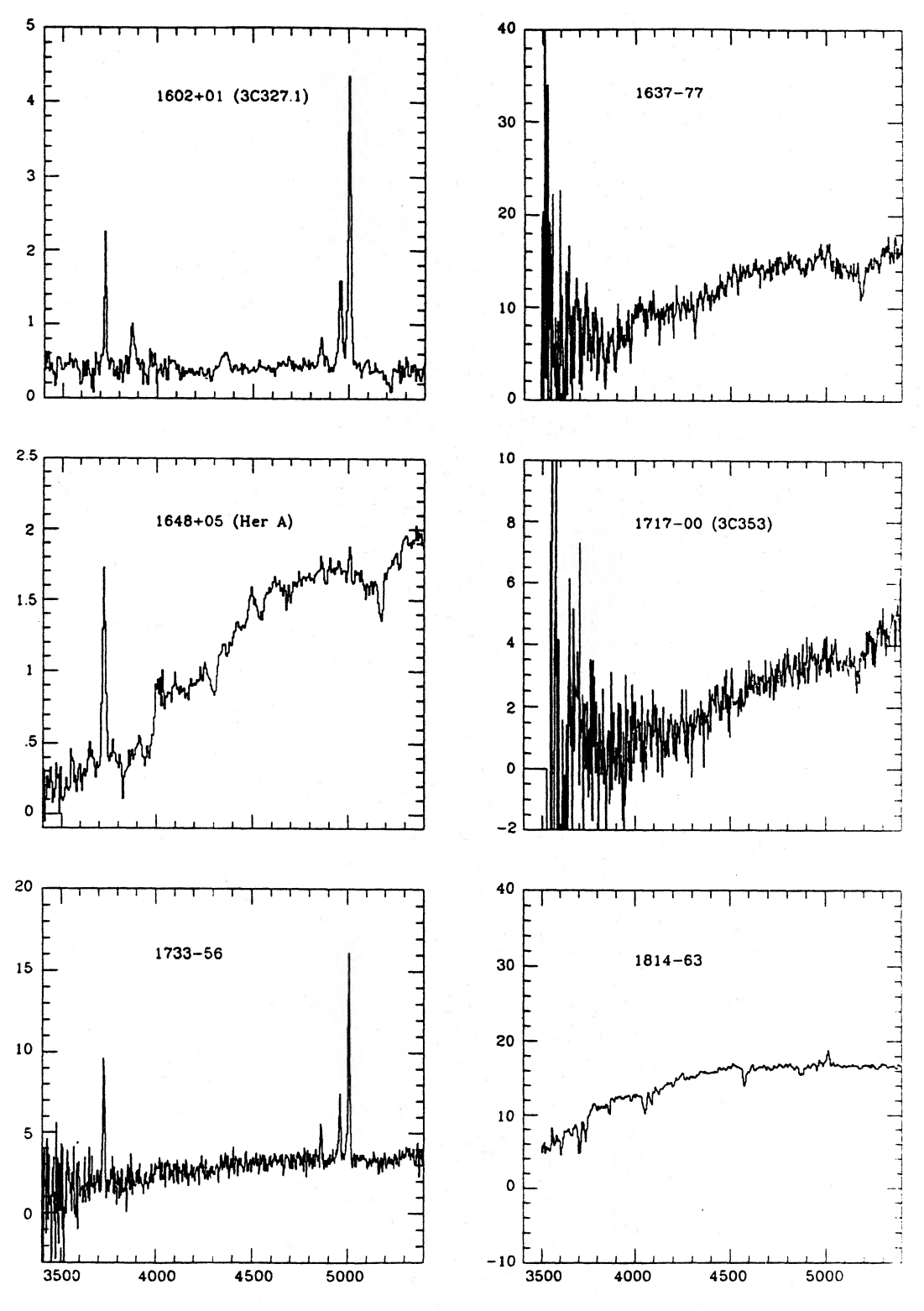


Figure 1 - continued

detected, but the continuum signal-to-noise ratio is relatively low.

0055 – 01 (3C 29). Weak $[O \, \text{III}] \lambda 5007$ and $H\beta$ emission lines are detected. The continuum colours appear similar to those of early-type galaxies, although the Ca II H & K absorption lines may be stronger than average.

0105 – 16 (3C 32). Rich, high-ionization emission-line spectrum. The continuum appears to be typical of early-type galaxies with Ca II H & K and Mg I absorption features detected.

0117 – 15 (3C 38). Rich, high-ionization emission-line spectrum. There is a marginal detection of a $Ca \, \Pi H$ absorp-

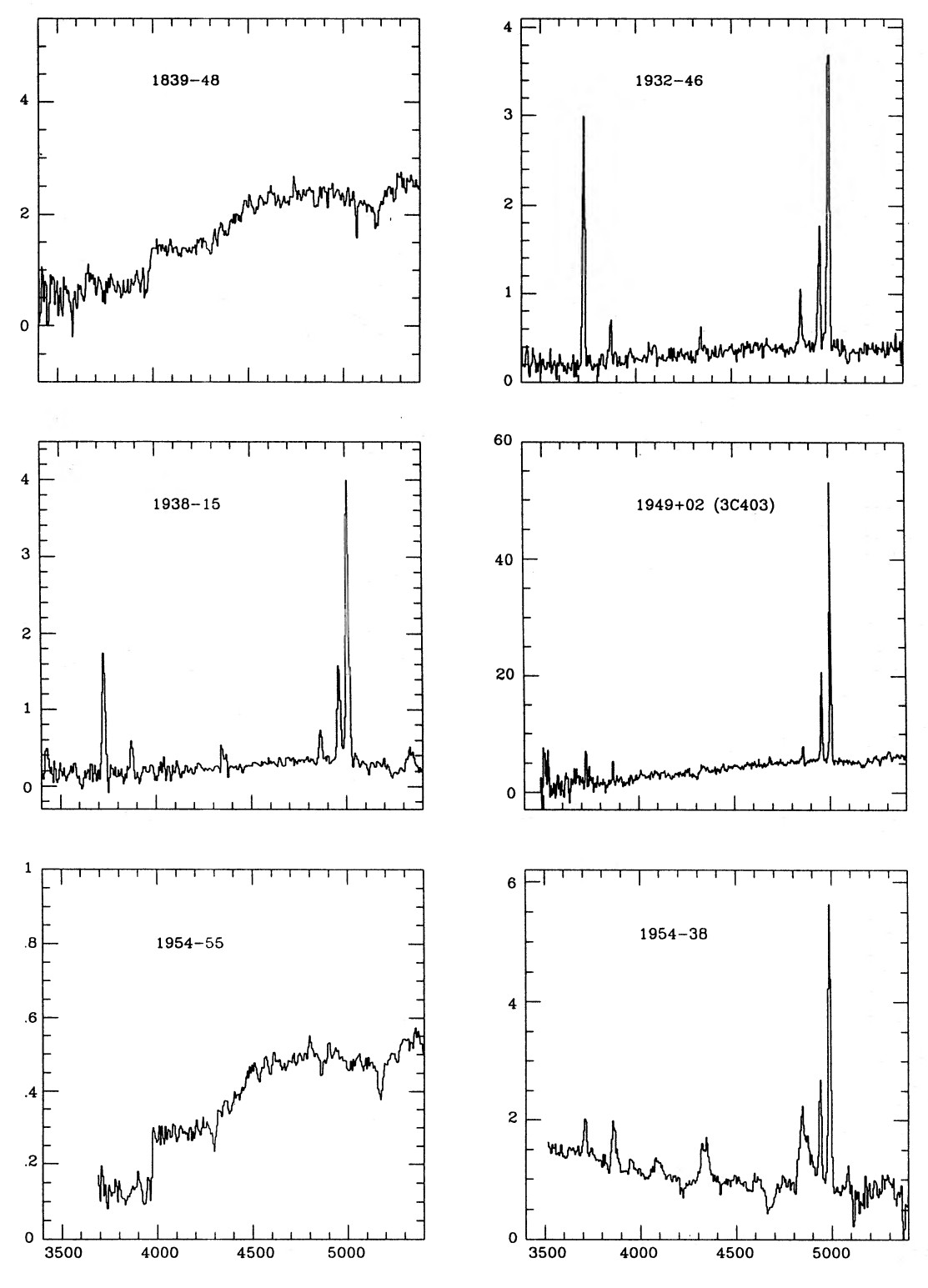


Figure 1 - continued

tion feature. The emission lines peak slightly off-nucleus in this object and are extended with evidence for velocity gradients. The value of $[O\ m]/H\beta$ given in Table 4 has been calculated using $H\gamma$ and assuming a case B recombination value for $H\gamma/H\beta$ (~ 0.45).

0123-01 (3C 40). No emission lines are detected from this object. The continuum appears typical of early-type galaxies.

0131-36 (NGC 612). Weak emission lines of $[O \, \text{III}] \lambda \lambda 5007$, 4959 and $[O \, \text{III}] \lambda 3727$ have been detected.

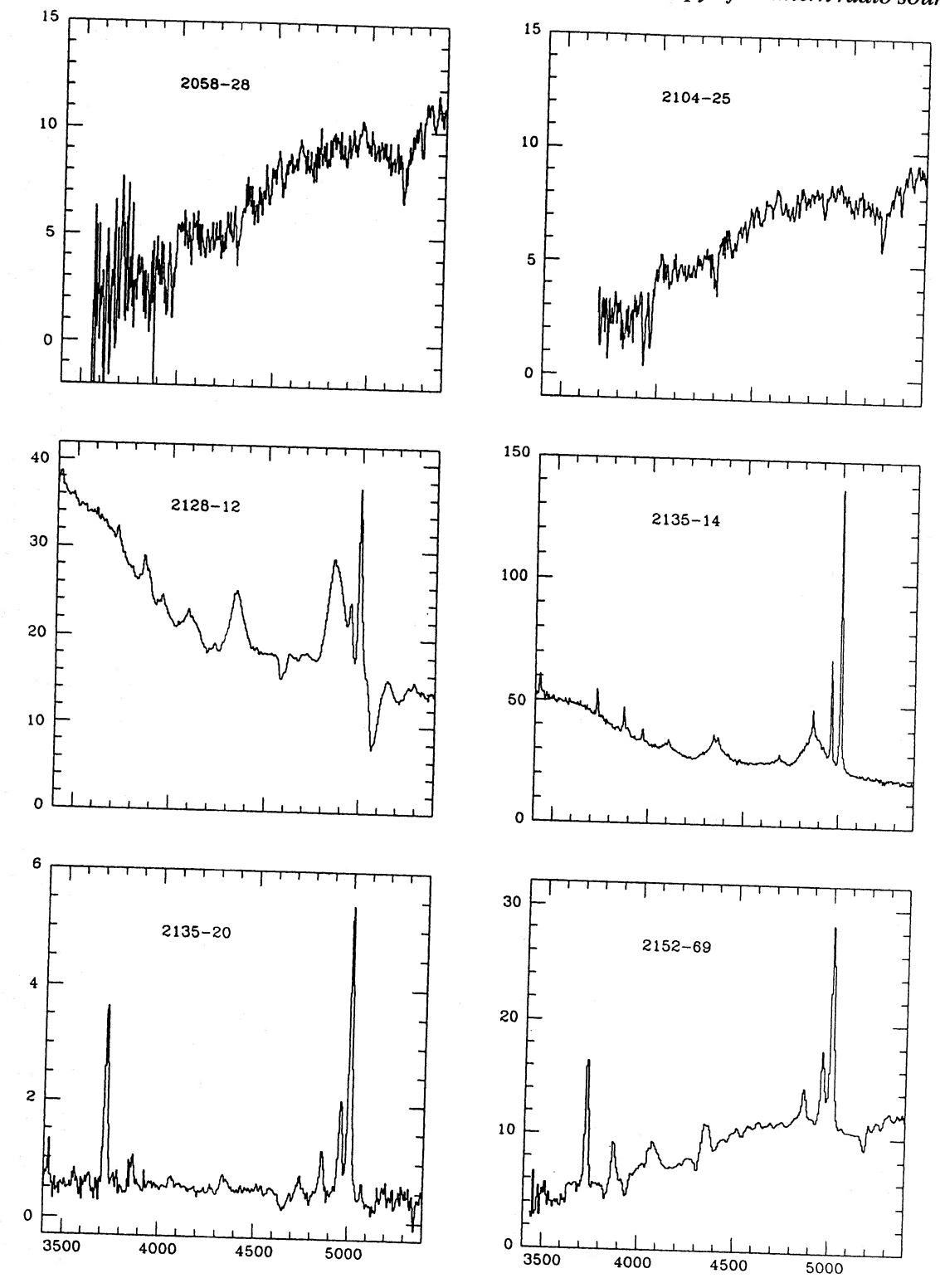


Figure 1 - continued

The continuum colours look to be typical of early-type galaxies, although the absorption features of Ca II H & K, H β and Na ID are unusually strong and narrow and the 4000-Å break appears to be weaker than average. The unusual absorption spectrum may be related to the disc structure of

the host galaxy, with the possibility of absorption by the interstellar medium in the disc.

0159 – 11 (3C 57). Quasar spectrum: strong, broad emission features (including Fe II blends), blue continuum, and relatively weak $[O III] \lambda\lambda 5007$, 4959 emission lines.

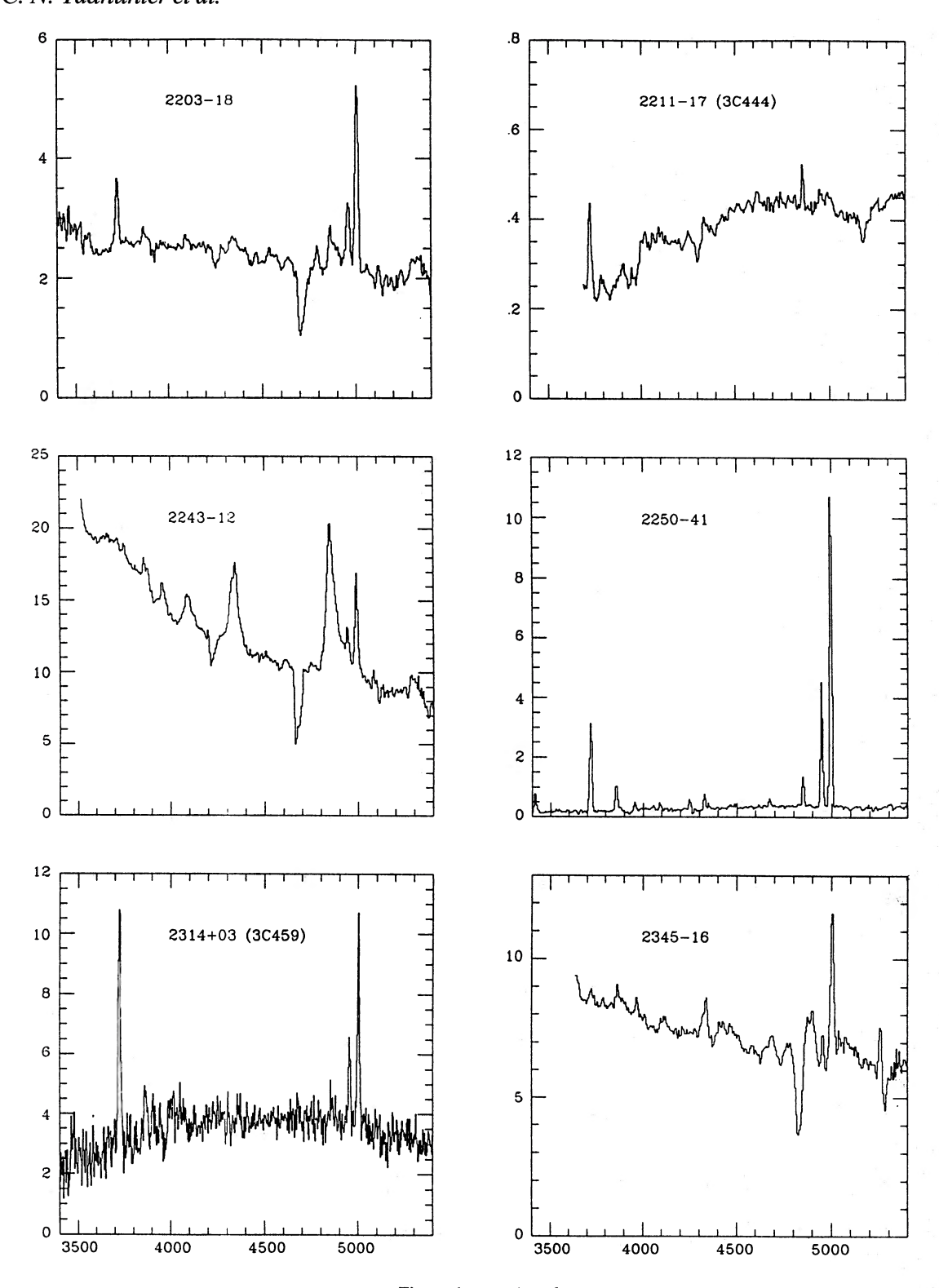


Figure 1 – continued

0213-13 (3C 62). Rich, high-ionization emission-line spectrum. The continuum appears typical of early-type galaxies.

0235 – 19. Rich, high-ionization emission-line spectrum. There are no clear detections of stellar absorption features.

0240 – 00 (NGC 1068). Rich, high-ionization emission-line spectrum. Extensively discussed elsewhere.

0252-71 ($\lambda < 4500$ Å only). Rich, high-ionization emission-line spectrum, no clear detections of stellar absorption features. Compact steep-spectrum radio source.

Table 2. Details of the objects in the *complete sample* observed in the survey. The third and fourth columns give the best available position, whose reference is listed in the fifth column: 1 = radio core position (see Paper II), 2 = optical position (see Section 5), 3 = WP85, 4 = Giles (1986), 5 = Fosbury et al. (1987). The sixth column gives the morphological classification from Wall & Peacock (1985) revised with our new data; the seventh column lists the redshifts, including the new ones.

Object	Other Name	R.A. h m s	Dec.	Ref.	Opt. Class.	Z
		16 116 8				
0023 - 26	OB-238	00 23 18.96	-26 18 49.5	1	G	0.322
0034 - 01	3C15	00 34 30.61	$-01\ 25\ 38.3$	2	G	0.073
0035 - 02	3C17	00 35 47.17	-02 24 09.3	2	G	0.220
0038 + 09	3C18	00 38 14.76	+09 46 59.5	1	G	0.188
0039 - 44		00 39 46.89	$-44\ 30\ 27.9$	2	G	0.346
0043 - 42		00 43 55.86	-42 24 14.6	2	G	0.116
0045 - 25	NGC253	00 45 05.74	-25 33 39.6	1	G	0.001
0055 - 01	3C29	00 55 01.57	-01 39 39.7	1	G	0.045
0105 — 16	3C32	01 05 48.74	-16 20 20.4	2	G	0.400
0117 - 15	3C38	01 17 59.66	-15 36 00.9	2	G	0.565
0123 - 01	3C40	01 23 27.49	-01 36 17.2	1	G G	0.018
0131 - 36	NGC612	01 31 43.50	-36 44 56.7	1 1	Q	0.030 0.669
0159 - 11 $0213 - 13$	3C57 3C62	01 59 30.34 02 13 12.35	-11 46 59.0 -13 13 25.4	2	G	0.147
0213 - 13 $0235 - 19$	OD-159	02 35 24.76	-19 45 30.8	2	G	0.620
0240 - 00	NGC1068	02 40 07.09	-00 13 30.7	3	Ğ	0.004
0252 - 71	11401000	02 52 26.65	-71 16 47.4	1	G	0.566
0255 + 05	3C75	02 55 03.01	+05 49 37.0	2	G	0.023
0305 + 03	3C78	03 05 49.09	+03 55 13.2	1	G	0.029
0320 - 37	For A	03 20 46.80	-37 23 06.0	3	\mathbf{G}	0.005
0325 + 02	3C88	03 25 18.19	+02 23 20.3	1	G	0.030
0349 - 27	OE-283	03 49 31.85	$-27\ 53\ 30.4$	3	G	0.066
0403 - 13	OF-105	04 03 13.95	$-13\ 16\ 18.4$	1	Q	0.571
0404 + 03	3C105	04 04 39.01	+03 34 27.4	2	G	0.089
0405 - 12	OF-109	04 05 27.46	$-12\ 19\ 31.9$	1	Q	0.574
0409 - 75		04 09 58.64	-75 15 04.7	2	G	0.693
0427 - 53		04 27 58.85	$-53\ 56\ 09.5$	1	G	0.038
0430 + 05	3C120	04 30 31.60	+05 15 59.5	3	G	0.033
0442 - 28	OF-271	04 42 37.81	-28 15 22.6	2	G	0.147
0453 - 20	OF-289	04 53 14.08	-20 38 58.9	2	G	0.035
0518 — 45	Pic A	05 18 23.54	-45 49 42.1	2	G	0.035
0521 - 36		05 21 12.94	-36 30 16.3	2	G G	0.055
0620 - 52		06 20 36.85	-52 40 00.9 -53 39 42.6	1 2	G	0.051 0.054
0625 - 53	OH-342	06 25 17.03 06 25 20.22	-35 27 22.0	2	G	0.055
0625 - 35 $0637 - 75$	OII-342	06 37 23.53	-75 13 37.2	2	Q	0.651
0736 + 01	OI61	07 36 42.53	+01 43 59.9	1	Ž	0.191
0806 - 10	3C195	08 06 30.29	-10 18 50.2	1	Ğ	0.110
0842 - 75	70100	08 42 11.52	-75 29 37.3	· 2	Q	0.524
0859 - 25	OJ-299	08 59 36.40	-25 43 26.0	2	Ğ	0.305
0915 - 11	Hyd A	09 15 41.19	$-11\ 53\ 04.9$	2	G	0.054
0945 + 07	3C227	09 45 06.54	+07 39 17.2	2	G	0.086
1136 - 13	OM-161	11 36 38.56	-13 34 05.5	2	Q	0.554
1151 - 34	OM-386	11 51 49.44	$-34\ 48\ 47.1$	1	Q	0.258
1216 + 06	3C270	12 16 49.90	+06 06 08.8	1	G	0.006
1226 + 02	3C273	12 26 33.25	+02 19 43.3	3	\mathbf{Q}	0.158
1246 - 41	NGC4696	12 46 03.27	-41 02 21.4	3	G	0.009
1251 - 12	3C278	12 51 58.56	$-12\ 17\ 52.2$	1	G	0.015
1253 - 05	3C279	12 53 35.84	$-05\ 31\ 08.1$	1	Q	0.538
1306 - 09	OP-10	13 06 02.09	-09 34 33.3	1	G?	0.464
1318 - 43	NGC5090	13 18 17.40	-43 26 33.4	1	G	0.011
1322 - 42	Cen A	13 22 31.47	-42 45 34.6	4	G	0.0018
1333 – 33	IC4296	13 33 47.16	-33 42 39.8	1	G	0.013
1355 – 41	0.0 4.5	13 55 57.20	-41 38 20.5	2	Q	0.313
1510 - 08	OR-107	15 10 08.90	-08 54 47.6	1	Q	0.361
1514 + 07	3C317	15 14 16.99	+07 12 17.1	1	G	0.035
1514 - 24	Ap Lib	15 14 45.27	-24 11 22.6	1	Q G	0.048
1547 — 79		15 47 39.43	-79 31 43.0	2	G	0.483

Table 2 - continued

Object	Other Name	R.A. h m s	Dec.	Ref.	Opt. Class.	, .
1549 — 79		15 49 28.07	-79 05 17.5	1	G	0.150
1559 + 02	3C327	15 59 55.64	+02 06 12.7	1	G	0.104
1602 + 01	3C327.1	16 02 12.96	+01 25 58.7	3	G	0.462
1637 - 77		16 37 05.10	-77 10 08.7	1	G	0.041
1648 + 05	Her A	16 48 39.99	+05 04 35.6	2	G	0.154
1717 - 00	3C353	17 17 53.28	$-00\ 55\ 48.7$	1	G	0.031
1733 - 56		17 33 21.43	-56 32 16.3	1	G G	0.098
1814 - 63		18 14 45.92	$-63\ 47\ 03.1$	1	G	0.063
1839 - 48		18 39 26.20	-48 39 23.1	1	G	0.112
1932 - 46		19 32 18.43	$-46\ 27\ 20.9$	2	G	0.231
1934 - 63		19 34 47.58	-63 49 37.8	5	G	0.183
1938 - 15	OV-164	19 38 24.60	-15 31 33.9	2	G	0.452
1949 + 02	3C403	19 49 44.51	+02 22 36.4	2	G	0.059
1954 - 55		19 54 18.15	-55 17 44.6	2	G	0.060
1954 — 38		19 54 39.05	-385313.3	1	Q	0.630
2058 - 28	OW-297.8	20 58 38.68	-28 13 43.9	1	G	0.038
2104 - 25	OX-208	21 04 29.87	$-25\ 37\ 50.2$	1	G	0.037
2128 - 12	OX-148	21 28 52.67	-12 20 20.6	1	Q	0.501
2135 - 14	OX-158	21 35 01.15	-14 46 27.4	1	- Q	0.200
2135 - 20	OX-258	21 35 01.33	$-20\ 56\ 03.7$	1	G	0.635
2152 - 69		21 52 58.01	-69 55 40.4	2	G	0.027
2203 - 18	OY-106	22 03 25.73	-185017.1	1	Q	0.618
2211 - 17	3C444	22 11 42.71	$-17\ 16\ 31.4$	2	G	0.153
2221 - 02	3C445	22 21 14.77	$-02\ 21\ 25.5$	2	G	0.057
2243 - 12	OY-172.6	22 43 39.79	-12 22 40.3	1	Q	0.630
2250 - 41		22 50 12.25	-41 13 44.4	2	G	0.310
2314 + 03	3C459	23 14 02.34	+03 48 55.0	1	G-	0.220
2345 - 16	OZ-176	23 45 27.68	-16 47 52.6	1	Q	0.576
-2356 - 61		23 56 29.58	$-61\ 11\ 41.6$	2	G	0.096

Table 3. Objects with good spectra in the literature that were not reobserved by us.

Object	Other Name	References
0349 - 27		Danziger et al. (1984), Tadhunter (1987)
0518 - 54	Pictor A	Carswell et al. (1984), Tadhunter (1987)
0521 - 36		Danziger et al. (1979), Tadhunter (1987)
0945 + 07	3C227	Osterbrock et al. (1976)
1322 - 42	Cen A	Phillips (1981)
1559 + 02	3C327	Penston & Fosbury (1978), Tadhunter (1987)
1934 - 63		Fosbury et al. (1987), Tadhunter (1987)
2221 - 02	3C445	Osterbrock et al. (1976), Tadhunter (1987)
2356 - 61		Tadhunter (1987), Danziger & Goss (1983)

0255+05 (3C 75). No emission lines are detected. The continuum appears to be typical of early-type galaxies.

0305+03 (3C 78). No emission lines are detected. The continuum appears to be typical of early-type galaxies.

0320-37 (Fornax A). No emission lines are detected. The continuum appears to be typical of early-type galaxies.

0325+02 (3C 88). Weak $[O\,\text{III}]\lambda5007$ is detected. The continuum appears typical of early-type galaxies (although the continuum signal-to-noise ratio is low).

0403 – 13 ($\lambda > 3800 \text{ Å}$ only). Quasar spectrum: broad Balmer emission lines are detected; blue continuum and $[O \text{ III}] \lambda \lambda 5007, 4959$ lines are also strong.

0404 + **03** (3C **105**). Strong [O III] $\lambda\lambda$ 5007, 4959 lines are detected, as well as weak H β . Curiously, [O II] λ 3727 is not detected. This may indicate an unusually high ionization state or a large reddening. The continuum colours appear typical of early-type galaxies, although there are no clear detections of stellar continuum features.

0405 – 12. Quasar spectrum: broad emission lines (including Fe II), blue continuum and relatively strong $[O III] \lambda\lambda 5007, 4959$ lines.

0409 – **75.** The emission lines $[O II] \lambda 3727$, $[Ne V] \lambda 3426$, $[Ne III] \lambda 3869$, $H\beta$ and $[O III] \lambda 5007$ have been detected. The feature at ~8340 Å is due to a poor signal-to-noise ratio,

Table 4. Emission-line fluxes, luminosities and ratios for the *complete sample*. In column 4 are listed the flux ratios between the wide and the narrow slit (see Section 6). The luminosities have been calculated assuming $H_0 = 50$ km s⁻¹ Mpc⁻¹ and $q_0 = 0$. The objects with galactic latitude $|b| < 25^{\circ}$ are indicated with an asterisk.

Object	Other Name	$\log F_{[OIII]}$ erg cm ⁻² s ⁻¹	W/N	$\begin{array}{c} \log L_{\rm [OIII]} \\ {\rm erg~s^{-1}} \end{array}$	$\log L_{{ m H}eta}({ m broad})$	[OIII]/[OII]	[OIII]/H <i>β</i>	
0023 - 26	OB-238	-14.38		42.41	_	0.75	2.47	
0034 - 01	3C15	-14.64		40.75		-	3.69	
0035 - 02	3C17	-14.09		42.32	_	1.50	4.86	
0038 + 09	3C18	-13.99		42.27	_	7.68	18.58	
0039 - 44	2010	-13.55		43.30	_	4.19	10.46	
0043 - 42		-14.85		40.96		4.20	-	
0045 - 25	NGC253	-14.14		37.50	÷_	-	0.47	
0055 - 01	3C29	-14.76		40.20	_	_	1.65	
0105 - 16	3C32	-14.37		42.63	_	3.28	10.95	
0117 15	3C38	-13.92		43.44	_	2.05	4.00	
0123 - 01	3C40	<-14.96		<39.20	-	-		
0131 - 36	NGC612	-14.58		40.03	_	_	3.14	
0159 - 11	3C57	-13.89		43.65	44.06	13.70	-	
0213 - 13	3C62	-13.68		42.36	-	4.52	15.30	
0235 - 19	OD-159	-13.95	0.85	43.50	-	9.68	10.03	
0240 - 00	NGC1068	-11.80	1.25	41.04	-	8.05	9.31	
0252 - 71		-14.98^a		42.38^{a}	-	_	-	
0255 + 05	3C75	<-15.10		<39.27	"-	_	-	
0305 + 03	3C78	<-15.10		<39.48	_	-	* _	
0320 - 37	ForA	<-14.10		<38.94	-	_	-	
0325 + 02	3C88	-14.77		39.83	-	·	_	
0349 - 27	OE-283	-13.95		41.35	<u>-</u>	0.59	6.90	
0403 - 13	OF-105	-14.14		43.24	43.25	_		
0404 + 03	3C105	-14.42		41.16	-	_	15.92	
0405 - 12	OF-109	-13.20		44.18	_	-	_	
0409 - 75		-15.28		42.71	_	0.57	_	
0427 - 53	9.0190	<-15.39	1.10	<39.43	40.00	- - 70	-	
0430 + 05	3C120	-12.54	1.16	42.15	42.03	5.72	0.65	
0442 - 28	OF-271	-13.96		42.08	-	1.54	9.65	
0453 - 20 $0518 - 45$	OF-289 PicA	<-15.22		<39.52	41.40	1 77		
0518 - 45 $0521 - 36$	FICA	-13.20 -13.99		41.54 41.16	41.40 41.11	1.77 3.13	4.21 5.47	
0621 - 50 $0620 - 52$		<-15.28		<39.78	-	5.15	0.41	
0625 - 53		<-15.46		<39.67		_	_	
0625 - 35*	ОН-342	<-15.18		<39.96	_	****	_	
0637 - 75	011 012	-13.65	1.18	43.87	43.44	>10.89	_	
0736 + 01*	OI61	-14.12	1.19	42.16	42.95	>12.49	_	
0806 - 10*	3C195	-12.82	1.97	42.95	_	8.53	12.64	
0842 - 75*		-13.86	1.79	43.42	44.03	_	_	
0859 - 25*		-14.69		42.01	_	1.16	3.18	
0915 - 11	HydA	-14.50		40.63	_	0.15	0.75	
0945 + 07	3C227	-13.39		42.15	42.0	12.67	9.01	
1136 - 13	OM-161	-13.39	1.13	43.95	43.71	12.48	_	
1151 - 34	OM-386	-13.95		42.62	42.48	4.33	19.61	
1216 + 06	3C270	<-14.64		<38.56	_	_	_	
1226 + 02	3C273	-12.62		43.48	44.25	>6.20	_	
1246 - 41*	NGC4696	<-15.03		<38.52	_	_	_	
1251 - 12	3C278	<-14.94		<39.05	_	_	_	
1253 - 05	3C279	-14.22		43.09	-	9.68	4.88	
1306 - 09	OP-10	-14.79		42.37	-	.—	2.20	
1318 - 43*	NGC5090	<-14.99		<38.73	-	_	_	
1322 - 42	Cen A	-		-		2.49	6.28	
1333 - 33	IC4296	<-14.76		<39.11		-		
1355 - 41*	-	-13.70		43.06	44.55	8.59	_	
1510 - 08	OR-107	-13.91	2.28	42.99	43.39	6.59	-	
1514 + 07	3C317	-14.38		40.37	-	0.37	3.13	
1514 - 24	ApLib	-14.65		40.37	-	0.56	4.13	
1547 - 79*		-13.68	1.63	43.51	_	9.20	8.41	
1549 - 79*		-13.73	0.97	42.33	-	11.22	14.85	

Table 4 - continued

Object	Other Name	$\log F_{[OIII]}$ erg cm ⁻² s ⁻¹	W/N	$log L_{[OIII]}$ erg s ⁻¹	$\log L_{{ m H}oldsymbol{eta}}({ m broad})$	[OIII]/[OII]	[ΟΙΙΙ]/H <i>β</i>
1559 + 02	3C327	-13.30		42.42	-	11.78	14.90
1602 + 01	3C327.1	-14.20	1.42	42.95		2.54	9.51
1637 - 77*		-14.15		40.73	_	1.06	9.61
1648 + 05	HerA	-15.26		40.81		0.22	
1717 - 00*	3C353	-14.94		39.70	-	_	0.92
1733 - 56*		-13.69	1.48	41.98	-	1.39	5.72
1814 - 63*		-14.45		40.82	_	-	-
1839 - 48*		<-16.22		<39.56	-	-	_
1932 - 46		-13.88	1.97	42.58	-	1.40	5.58
1934 - 63		-14.00		42.24	-	4.17	7.07
1938 - 15*	OV-164	-14.22	1.02	42.90	_	2.92	9.27
1949 + 02*	3C403	-13.30	1.30	41.91	-	8.41	20.10
1954 - 55		<-16.00		<39.19	-	_	
1954 - 38		-14.12	1.53	43.36	43.04	6.97	_
2058 - 28	OW-297.8	-15.08		39.74	-	_	1.03
2104 - 25	OX-208	-14.66		39.83	-	-	,
2128 - 12	OX-148	-13.56		43.68	44.15	12.09	-
2135 - 14	OX-158	-12.99	1.12	43.33	43.39	11.74	10.42
2135 - 20	OX-20	-14.10	1.16	43.38	-	2.78	7.46
2152 - 69		-13.42		41.09	-	2.47	7.42
2203 - 18	OY-106	-14.37		43.09	_	2.26	2.93
2211 - 17	3C444	-15.44		40.63	-,	0.25	0.57
2221 - 02	3C445	-12.76		42.41	41.95	14.10	12.89
2243 - 12	OY-172	-14.14	1.08	43.34	44.08	10.38	
2250 - 41		-13.80	1.00	42.95	,-	4.41	11.29
2314 + 03	3C459	-14.01	1.37	42.40		0.68	8.53
2345 - 16		-14.25		43.13	>43.17	7.53	-
2356 - 61		-13.42		42.22	· <u>-</u>	2.65	12.62

^{*}Objects with galactic latitude $|b| < 25^{\circ}$. $^{a}[O II]$ flux and luminosity.

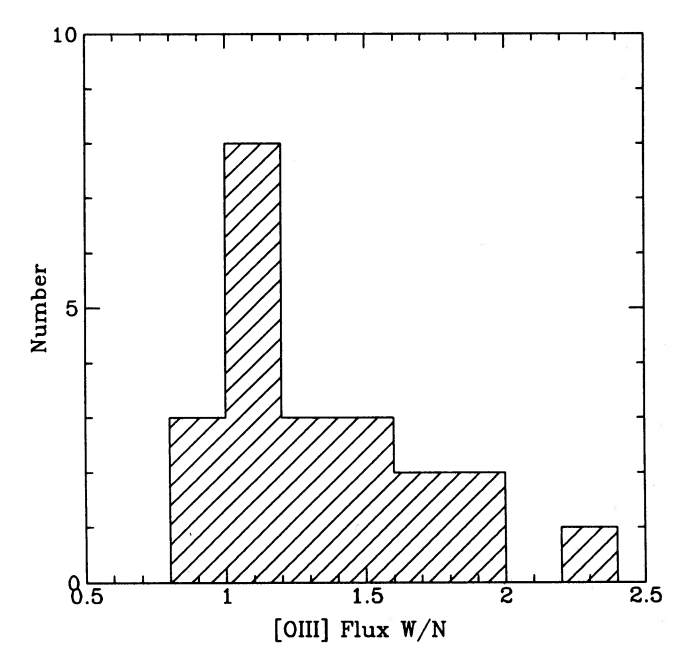


Figure 2. Histogram showing the distribution of the ratio of the wide/narrow-slit $[O \, II]$ fluxes for the objects in which both measurements were available.

bad sky subtraction and fringing. The $[O \, \text{III}] \lambda 5007$ is unusually weak for a radio galaxy of this power and redshift. The $[O \, \text{II}] \lambda 3727$ line is clearly extended.

0427-53 (0428-53 in WP85). No emission lines are detected from this object. The continuum spectrum appears typical of early-type galaxies.

0430 + 05 (3C 120). Broad-line radio galaxy, extensively studied. Quasar-like spectrum: broad Balmer and Fe II lines/blends, strong $[O \, \text{III}] \, \lambda \lambda 5007$, 4959 lines, blue continuum.

0442 – 28. Strong $[O \, \text{III}] \lambda \lambda 5007$, 4959 and $[O \, \text{III}] \lambda 3727$ emission lines are detected. The continuum colours may be slightly bluer than those of typical early-type galaxies, and there are no clear detections of stellar absorption features (but the continuum signal-to-noise ratio is low).

0453 – 20. No emission lines are detected. The continuum spectrum appears typical of early-type galaxies.

0620 – **52.** Weak $H\alpha + [N II]$ is detected, but no $[O III] \lambda 5007$ or $[O II] \lambda 3727$. The continuum spectrum appears typical of early-type galaxies.

0625-53. No emission lines are detected. The continuum colours appear bluer than the average early-type galaxy. The Mg1b absorption feature is detected.

0625 – **35.** Weak H α + [N II] is detected, but no [O III] λ 5007 or [O II] λ 3727. The continuum colours are typical of early-type galaxies.

- **0637 75.** Quasar spectrum: broad Balmer lines, blue continuum, and $[O \text{ III}] \lambda \lambda 5007$, 4959 lines of moderate equivalent width.
- 0736+01. Quasar spectrum: strong, broad Balmer and Fe II lines, blue continuum, and $[O III] \lambda 5007$ lines of moderate equivalent width. The [O III] line may be contaminated by Fe II emission.
- 0806 10 (3C 195). Rich, high-ionization emission-line spectrum. The continuum spectrum is typical of early-type galaxies. The emission lines are clearly extended in this object.
- **0842 75.** Quasar spectrum: strong, broad Balmer lines and $[O III] \lambda 5007$ (note that $[O III] \lambda 5007$ falls on atmospheric A band), blue continuum. The $[O III] \lambda 5007$ flux in Table 4 is taken as 3 times the $[O III] \lambda 4959$ flux. The emission lines may be extended in this object.
- **0859 25.** Emission lines of $[O III] \lambda\lambda 5007$, 4959 and $[O II] \lambda 3727$ are detected. Moderate ionization state. The continuum appears typical of early-type galaxies.
- **0915–11** (Hydra A). weak $[O III] \lambda 5007$ and moderate $[O II] \lambda 3727$ are detected. The continuum appears typical of early-type galaxies.
- 1136 13. Quasar spectrum: broad Balmer lines and rich, high-ionization narrow-line spectrum, blue continuum. The emission lines are clearly extended in this object.
- 1151-34. Spectrum characteristic of broad-line radio galaxies: rich, high-ionization narrow-line spectrum, strong, highly structured Balmer lines, and blue continuum. Compact steep-spectrum radio source.
- **1216+06** (3C **270**). Weak $H\alpha + [NII]$ is detected, but no $[OIII]\lambda 5007$ or $[OIII]\lambda 3727$. The continuum spectrum is typical of early-type galaxies.
- 1226+02 (3C 273). Quasar spectrum, extensively studied: strong, broad Balmer and Fe II lines, blue continuum, $[O III] \lambda 5007$ of small equivalent width. $[O III] \lambda 5007$ may be contaminated by Fe II emission.
- **1246 41 (NGC 4696).** Weak H α + [N II] is detected, but no [O III] λ 5007 or [O II] λ 3727. The continuum spectrum is typical of early-type galaxies.
- 1251 12 (3C 278). Weak $H\alpha + [N II]$ is detected, but no $[O III] \lambda 5007$ or $[O III] \lambda 3727$. The continuum spectrum is typical of early-type galaxies.
- 1253 05 (3C 279). BLLac spectrum: $[O III] \lambda 5007$ of small equivalent width detected close to atmospheric Aband. The continuum is relatively blue and featureless (most of the structure is due to atmospheric absorption features).
- 1306 09 ($\lambda > 3850$ Å only). Emission lines $[O \text{ III}] \lambda\lambda 5007$, 4959 and H β are detected. The excitation is only moderate. The information about the continuum is limited, but the Ca II H line is marginally detected. Compact steep-spectrum radio source.
- 1318 43 (NGC 5090). Weak H α + [N II] is detected, but no [O III] λ 5007 or [O II] λ 3727. The continuum spectrum is typical of early-type galaxies.
- 1333 33 (IC 4296). Weak $H\alpha + [N II]$ is detected, but no $[O III] \lambda 5007$ or $[O II] \lambda 3727$. The continuum spectrum is typical of early-type galaxies.
- 1355 41. Quasar spectrum: strong, broad Balmer lines, blue continuum and $[O \text{ III}] \lambda \lambda 5007$, 4959 lines of moderate strength.
 - 1514 24 (Ap Lib). BL Lac spectrum: $[O III] \lambda 5007$ and

- $[O II] \lambda 3727$ lines of small equivalent width. The continuum is blue, but the Mg I b absorption feature is detected.
- 1547 79. Rich, high-ionization emission-line spectrum. There are no clear detections of stellar absorption features (but the signal-to-noise ratio is low). The emission lines may be slightly extended.
- 1549 79. Rich, high-ionization emission-line spectrum. The 'narrow' emission lines are relatively broad. The continuum colours are typical of early-type galaxies, with Mg 1b, Ca II H & K and the G-band stellar absorption features detected. Compact radio source.
- **1602 + 01 (3C 327.1).** Rich, high-ionization emission-line spectrum. The emission lines may be slightly extended.
- 1637 77. Weak [O II] λ 3727 and [O III] λ 5007 emission lines are detected. The ionization state is moderate. The continuum spectrum is typical of early-type galaxies.
- 1648+05 (Hercules A). This object has two diffuse continuum components separated by 3 arcsec. Moderate $[O\,\textsc{ii}]\,\lambda3727$ and weak $[O\,\textsc{iii}]\,\lambda5007$ are detected in one of the two components. Both components show an absorption-line spectrum typical of early-type galaxies. The $[O\,\textsc{ii}]$ emission is extended.
- 1717 00 (3C 353). Weak $[O\,\text{m}]\lambda 5007$ and $H\alpha$ emission lines are detected. The ionization state is low. The continuum colours appear typical of early-type galaxies, and a Mg Ib absorption feature is detected.
- 1733 56. Emission spectrum of moderate ionization. The continuum colours may be slightly bluer than is typical of early-type galaxies, and there are no clear detections of stellar absorption features (but the signal-to-noise ratio is low).
- 1814-63. [O III] λλ5007, 4959 emission lines are detected. The spectrum of this object is strongly contaminated by the light from a nearby star, and the continuum features apparent in Fig. 1 are due to this star. Therefore we have no information about the continuum in this object. Compact steep-spectrum radio source.
- 1839 48. No emission lines detected from this object. The continuum is typical of an early-type galaxy.
- 1932 46. Rich emission-line spectrum of moderate ionization. There are no clear detections of stellar absorption features (but the signal-to-noise ratio is low).
- 1938 15. Rich, high-ionization emission-line spectrum. No clear absorption features have been detected (but the signal-to-noise ratio is low).
- 1949+02 (3C 403). High-ionization emission-line spectrum. The emission lines appear unusually narrow. The continuum colours are typical of early-type galaxies, with Mg1b and G-band absorption features detected.
- **1954 55.** Weak $H\alpha + [N II]$ is detected, but no $[O III] \lambda 5007$ or $[O II] \lambda 3727$. The continuum spectrum is typical of early-type galaxies.
- 1954 38. Quasar spectrum: strong, broad Balmer lines, blue continuum and $[O \text{ III}] \lambda\lambda 5007$, 4959 lines of large equivalent width.
- **2058 28.** Weak $[O \text{ III}] \lambda 5007$ and H β emission lines of comparable strength are detected. Low ionization state. The continuum spectrum is typical of early-type galaxies.
- **2104 25.** Weak $[O III] \lambda 5007$ emission line is detected. The continuum colours appear similar to early-type galaxies, but the Ca II H & K lines are unusually strong.
 - 2128 12. Quasar spectrum: broad Balmer lines, blue

continuum and $[O III] \lambda \lambda 5007$, 4959 lines of moderate equivalent width are detected.

2135 – 14. Quasar spectrum: broad Balmer lines, blue continuum and $[O \text{ III}] \lambda\lambda 5007$, 4959 lines of large equivalent width are detected.

2135 – 20. Rich, moderate-ionization emission-line spectrum. No stellar absorption features have been clearly detected. Compact steep-spectrum radio source.

2152–69. Rich, moderate-ionization emission-line spectrum, broad wings have been detected to the Balmer lines. The continuum spectrum is typical of early-type galaxies. This object has a bright emission-line blob, ~ 10 arcsec to the NE of the nucleus: see Tadhunter et al. (1988) for a detailed discussion of this object. The emission-line fluxes in Table 4 refer only to the line emission associated with the core of the galaxy.

2203 – 18. Quasar spectrum: broad Balmer lines, blue continuum and $[O III] \lambda\lambda 5007$, 4959 lines of moderate equivalent width.

2243 – 12. Quasar spectrum: strong, broad Balmer lines, blue continuum and $[O III] \lambda\lambda 5007$, 4959 lines of small equivalent width.

2250 – 41. Rich, high-ionization emission-line spectrum. Mg1b and G-band absorption features are detected at a marginal level. This object has a luminous extended emission-line region, 7 arcsec to the west of the core. The emission-line fluxes in Table 4 only refer to the line emission associated with the core.

2314 + 03 (3C 459). Emission-line spectrum of moderate ionization. The continuum spectrum is bluer than a typical early-type galaxy, and absorption features suggestive of young stellar populations have been detected.

2345 – 16. Quasar spectrum: broad Balmer lines, blue continuum and $[O \text{ III}] \lambda\lambda 5007$, 4959 lines of moderate equivalent width.

8 CONCLUSIONS

We have presented new spectroscopic observations for a complete sample of 87 radio sources selected from the WP85 2-Jy catalogue with redshifts z < 0.7 and declinations $\delta < +10^{\circ}$.

To ensure the completeness of the sample, we have also observed most of the objects for which no spectroscopic redshift was given in PW85: of the newly obtained redshifts, 19 fall within our z < 0.7 sample (see Paper III). Although 14 objects remain without redshift, we are now confident that our final z < 0.7 sample is largely complete.

With the new observations we have obtained a homogeneous data set for all the objects in the sample. Along with measurements (or limits) of the $[O \ III] \lambda 5007$ fluxes for all the objects, we have also obtained $[O \ II] \lambda 3727$ fluxes in 47 cases and H β fluxes in 40 cases. These measurements can be used

to construct useful emission-line diagnostics. New radio data were collected for the objects in the complete sample, and they are presented in Paper II. The full set of data will be the basis for a discussion of the properties of radio-loud active nuclei, which will be presented in a forthcoming paper (Paper IV).

ACKNOWLEDGMENTS

We thank the ESO time allocation committee for their generous support of this project, and the technical staff at La Silla for four near-flawless runs.

REFERENCES

Barthel P. D., 1989, ApJ, 336, 606

Baum S. A., Heckman T., 1989a, ApJ, 336, 681

Baum S. A., Heckman T., 1989b, ApJ, 336, 702

Baum S. A., Heckman T., Bridle A. H., van Breugel W., Miley G., 1988, ApJS, 68, 643

Carswell R. F., Baldwin J. A., Atwood B., Phillips M. M., 1984, ApJ, 286, 464

Danziger I. J., Goss W. M., 1983, MNRAS, 202, 703

Danziger I. J., Fosbury R. A. E., Goss W. M., Ekers R. D., 1979, MNRAS, 188, 415

Danziger I. J., Fosbury R. A. E., Goss W. M., Bland J., Boksenberg A., 1984, MNRAS, 208, 589

Fosbury R. A. E. et al., 1987, MNRAS, 225, 761

Giles A. B., 1986, MNRAS, 218, 615

Heydari-Melayeri M., Jarvis B., Gillotte A., 1989, ESO Operating Manual No. 9, ESO Publications

Hine R. G., Longair M. S., 1979, MNRAS, 188, 111

Jackson N., Browne I. W. A., 1990, Nat, 343, 43

Lasker B. M., Sturch C. R., McLean B. J., Russell J. L., Jenkner H., Shara M. M., 1990, AJ, 99, 2019

Melnick J., Dekker H., D'Odorico S., 1989, ESO Operating Manual No. 4, ESO Publications

Morganti R., Ulrich M.-H., Tadhunter C. N., 1992, MNRAS, 254, 546

Morganti R., Killeen N., Tadhunter C. N., 1993, MNRAS, 263, 1023 (Paper II, this issue)

Orr M. J. L., Browne I. W. A., 1982, MNRAS, 200, 1067

Osterbrock D. E., Koski A. T., Phillips M. M., 1976, ApJ, 206, 898

Penston M. V., Fosbury R. A. E., 1978, MNRAS, 183, 479

Phillips M. M., 1981, MNRAS, 197, 659

Rawlings S., Saunders R., 1991, Nat, 349, 138

Rawlings S., Saunders R., Eales S. A., Mackay C. D., 1989, MNRAS, 240, 701

Saunders R., Baldwin J. E., Rawlings S., Warner P. J., Miller L., 1989, MNRAS, 238, 777

Schmidt M., 1965, ApJ, 141, 1

Schwarz H. E., Melnick J., 1989, ESO User Manual, ESO Publications

Tadhunter C. N., 1987, D.Phil. thesis, Univ. Sussex

Tadhunter C. N. et al., 1988, MNRAS, 235, 403

Wall J. V., Peacock J. A., 1985, MNRAS, 216, 173 (WP85)

Yee H. K. C., Oke J. B., 1978, ApJ, 226, 753